RSC Advances

ROYAL SOCIETY
OF **CHEMISTRY**

www.rsc.org/advances

1

Influence of the Ce₂O₃ and CeO₂ promoters on the Pd / MgO catalyst in dry-reforming of methane

Faris A. J. Al-Doghachi[a,b], Umer Rashid[c], Zulkarnain Zainal[a,b], Mohd Izham Saiman[a,b] and Yun Hin Taufiq Yap[a,b*]

[a]Catalysis Science and Technology Research Centre, Faculty of Science, Universiti Putra Malaysia, 43400, UPM, Serdang, Selangor, Malaysia.

[b]Department of Chemistry, Faculty of Science, Universiti Putra Malaysia, 43400 UPM Serdang, Selangor, Malaysia.

[c]Institute of Advanvced Technology, Universiti Putra Malaysia, 43400 UPM Serdang, Selangor, Malaysia.

*Corresponding author:

Prof. Dr. Yun Hun Taufiq-Yap
Catalysis Science and Technology Research Centre
Faculty of Science, Universiti Putra Malaysia, 43400 UPM Serdang,
Selangor, Malaysia.
Email: taufiq@upm.edu.my
Tel: + 60-3-89466809; Fax: + 60-3-89466758

2

Abstract

In this study, the conversion of methane and CO_2 to synthesis gas using dry reforming over Pd/MgO catalysts in different concentrations of Ce^{3+} and Ce^{4+} was investigated. Besides that, it was also examined the factors that contribute to the deposition of carbon during co-precipitation method. The catalysts used in this study, were prepared using K_2CO_3 as the precipitant. The characterization of the catalysts were performend using stete-of-the-art techniques *i.e.* XRD, XPS, FT-IR, TPR-H_2, BET, TEM, FE-SEM, and TGA. It was found that with the addition of Ce promoter, the catalyst Pd/$Mg_{0.85}Ce_{015}O$ appraised a high level of activity (CH_4; 54%, and CO_2; 74%) and with excellent stability. The results of this analysis also revealed an outstanding anti-coking activity of reduced catalyst with low Pd metal. Additionally,we have studied the catalyst performance and stability of the produced catalyst.

Keywords: Biogas, Dry reforming, Catalyst deactivation, Synthesis gas, H_2 production.

3

1. Introduction

The production of biogas (CO_2 and CH_4) from the anaerobic digestion of biomass (fermented wastes) has directly exploited as fuel for small-to-medium-scale combined heat production as well as power production. It has also used as a renewable carbon source in the production of synthesis gas (syngas) (CO and H_2) for industrial feedstock through an economically and environmentally friendly reaction.[1] The alternative method to this energy intensive process is to use of steam reforming of methane, which, is a well-established production route, as in Eq. 1.[2] or the use of carbon dioxide as an oxidant in the commonly known as 'dry reforming process', as in Eq. 2.

$$CH_4 + H_2O \longrightarrow 3H_2 + CO \quad \Delta H^o_{298^oK} = +225.4 \text{ kJ/mol} \tag{1}$$

$$CH_4 + CO_2 \longrightarrow 2H_2 + 2CO \quad \Delta H^o_{298^oK} = +247.3 \text{ kJ/mol} \tag{2}$$
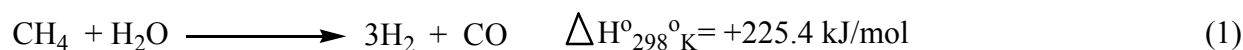
Syngas is a vital feedstock which can be effectively converted to ultra clean fuels, such as methanol, gasoil, gasoline, and dimethyl ether (DME), through the use of Fischer–Tropsch synthesis.[3] The equilibrium of the reaction during the production of syngas from CH_4 and CO_2 (Eq. 2), is affected by the simultaneous reaction of reverse water-gas shift (RWGS) (Eq. 3). The resulting effect is a low H_2/CO ratio.

$$CO_2 + H_2 \longrightarrow H_2O + CO \quad \Delta H^o_{298^oK} = +41.2 \text{ kJ/mol} \tag{3}$$

Also, the dry reforming reaction is associated with other side reactions, such as the decomposition of methane (Eq. 4), as well as the disproportionation reaction (Boudouard reaction) (Eq. 5).

$$CH_4 \longrightarrow C + 2H_2 \quad \Delta H^o_{298^oK} = +75.3 \text{ kJ/mol} \tag{4}$$

$$2CO \longrightarrow C + CO_2 \quad \Delta H^o_{298^oK} = -171 \text{ kJ/mol} \tag{5}$$

4
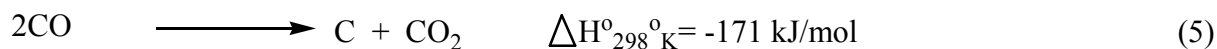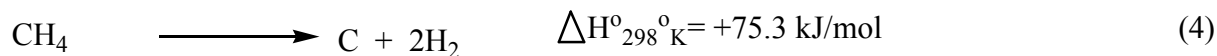
Zhang et al.[4] reported that CH_4 decomposition (Eq. 4) and CO disproportionation (Eq. 5) have shown a direct relation to the carbon deposition on the catalyst. When the temperature of the reaction increases from 550 $^{\circ}$C to 650°C, the observation revealed that a higher tendency for the deposition of carbon rather than the DRM. Thus, the choice of catalyst selected plays a crucial role in the prevention of carbon formation and at the same time it also improves the reaction of DRM. Furthermore, the deposition of carbon can be reduced or even eliminated through the support of metal on a metal oxide (MO) with a strong basicity.[5] This occurs because an increase in the basicity of the support causes the catalyst to chemisorb CO_2 in the CO_2 reforming of methane. Consequently, these species react with C to form CO (Eq. 6).

$$CO_{2(g)} + C_{(s)} \longrightarrow 2CO_{(g)} \tag{6}$$

It is an important to consider the two remarkably significant factors in the design of the anti-carbon deposition catalysts, the first factor is the deposition of carbon that can only take place when the metal cluster is greater than the critical size. The other factor is carbon deposition that is favored by acidic support. Thus, it is obvious that the size of the metal cluster must be smaller than the critical size which required for coke formation in order to prevent the deposition of the carbon, also, the acidity of the support must be reduced too. Thus, the best way to reduce the acidity, is to select the basic metal oxides as in an alkaline earth metal oxides, that can function as effective support.[6] The selection of MgO as a support lies in its properties that allow for the prevention of acidity and control in the size of the Ni particles, through the use of small amounts of NiO. This is one way to prevent the deposition and sintering of the carbon. The other two factors, that have encouraged the researchers in the selection of MgO as a support include high thermal stability with a high melting point of 2850 $^{\circ}$C, and its cost of production is rather low.[7]

5

It is evident that the performance of supported catalysts can be easily improved by the selection of proper promoting materials. It has also been found that supported transition metals, particularly Ni, Ru, Rh, Pd, and Ir have considerable effects on reforming reactions. It has been reported that noble metals are more active but with less sensitivity to coking. However, supported nickel is the preferred choice; hence it is used more frequently in industrial reforming processes since it is easily available and its cost is low.[8,9] Seshan et al.[10] performed evaluations of several catalytic formulations with Ni or Pt supported on ZrO_2. The findings revealed Pt/ZrO_2 to be a very stable catalyst throughout the reaction, in comparison to the Ni- based catalyst[11]

The use of alkaline promoters, such as CaO, can prevent sintering efficiently. Dias and Assaf[12] found out that when calcination occurs, sintering can cause deactivation during the preparation of catalysts. Recently, Juan-Juan et al.[13] examined the benefits of the addition of potassium to the catalyst. It was found that the pre-treating of nickel species with hydrogen could further reduce the nickel species. Likewise, Luna and Iriarte[14], who discovered that the addition of potassium could prevent the accumulation of carbon on the surface of the catalyst. Numerous studies[15,16] have reported that CeO_2 can store and release a large amount of oxygen reversibly in response to the gas phase concentration. This feature is referred to as Oxygen Storage Capability (OSC). Although there have been extensive studies on MgO, ZrO_2 and Al_2O_3, as catalyst promoters, there is little investigations on the use of Ce^{3+} and Ce^{4+} as a promoter of Pd/MgO for DRM[17].

The use of ceria is much preferred because of its high oxygen storage/transport capacity. In fact, ceria plays a significant role as a promoter in DRM reactions, due to its ability to supply oxygen from its lattice and to replace oxygen with support through the dissociation of CO_2 on its surface[18]. The adsorption and activation of CO_2 take place on the surface sites of Ce^{3+} while CO

is formed and Ce^{3+} is oxidized to Ce^{4+} simultaneously. As, ceria can chemisorb large amounts of H_2 and CO, its intake depends on the thermal treatment conditions and surface/bulk properties of ceria[19]. Besides the effects of ceria as a promoter on the dissociative adsorption of CO_2, it is capable of enhancing the stabilization and dispersion of small metal particles. This can lead to significant changes to the surface features of both metal and oxide [20]. Therefore, it is postulated that the occurrence of high thermal stability in dispersed metal, as well as the formation of Ce–M alloys in a reductive atmosphere is due to effects of Strong Metal-Support Interaction (SMSI). Since, SMSI reduces catalytic activity, bulk Ce_2O_3 is not a proper support for nickel. Recently, many research studies employed on DRM to develop improved Ce with ternary and binary supports[21,22].

Thus, the present research is aimed to investigate the effects of Ce^{3+} and Ce^{4+} as a promoter on MgO, which acts as a carrier and also the effects of doping the Pd metal on the surface of the support. The comparison on the activity and stability of the promoter catalysts and non-promoter Pd/MgO catalyst was done for better understanding of the effects of the promoter on the catalytic performance during DRM reaction. The catalysts were also characterized by the chemical analysis, nitrogen adsorption desorption measurements, XRD, XPS, FT-IR, HRTEM, BET, TGA and FE-SEM-EDS.

2. Experimental

2.1. Catalysts preparation

The catalysts $Mg_{1-x}Ce^{3+}_xO$ (x = 0.00, 0.03, 0.07, 0.15) were prepared using the co-precipitation method.[23] Meanwhile, the support MgO and promoter Ce_2O_3 were prepared using 0.1M aqueous solution of $Ce(NO_3)_3.6H_2O$ (Merck; >99.0%) and $Mg(NO_3)_2.6H_2O$ (Merck; >99.0%) and 1M

K_2CO_3 (Merck; >99.7%), which were used as precipitants. The sample was rinsed with hot water after the filtration of the precipitant. Then, the sample was dried at 120^oC for 12 h. Subsequently, it was pre-calcined in air at 500^oC for 5h to remove CO_2 from the precipitant. After that, the sample was pressed into disks at 600 kg/m^2, followed by calcination at 1150^oC for 20 h for enhancement of the mechanical properties and for ensuring good interaction between the support, MgO and the promoter Ce_2O_3.

Table 1 shows the preparation of the catalyst. Initially, 1% Pd was impregnated using $Pd(C_5H_7O_2)_2$ (Aldrich; >99%) which was dissolved with dichloromethane. After impregnation in the air, the catalysts were dried for 12 h at a temperature of 120^oC. The dried catalysts were sieved before grinding them into particles of 80–150 or 150–250μm in diameter. The same process was applied for the $Pd/Mg_{1-x}Ce^{4+}_xO$ ($x = 0.03, 0.07, 0.15$) catalysts. The only change was the $Ce(NO_3)_3.6H_2O$ salt replaced with the $(NH_4)_2Ce(NO_3)_6.6H_2O$ salt.

2.2. Catalyst characterization

The thermogravimetric analysis (TGA) was accomplished on a Mettler Toledo TG-DTA Apparatus (Pt crucibles, Pt / Pt − Rh thermocouple) with a purge gas (nitrogen) flow rate of 30 ml min^{-1} and a heating rate of 10 °C/min from 50 to 1000 °C.

The XRD analysis was performed using a Shimadzu diffractometer (XRD 6000). The diffractometer used Cu-Kα radiation at ambient temperature to get diffraction patterns from powder crystalline samples. The Cu-Kα radiation was obtained by Philips glass diffraction X-ray tube broad focus 2.7KW type. The samples size D crystallite were measured using the Debye–Scherrer's relationship[24]. Where, D is the crystalline size, λ is the incident X-ray wavelength, β is the full width at half-maximum (FWHM), and θ is the diffraction angle.

8

The Fourier transform infrared (FT-IR) analysis was conducted on PerkinElmer spectrometer model 100 series (sample preparation UATR).

The total catalyst surface area was obtained with nitrogen gas adsorption at −196 °C, using Brunauer–Emmett–Teller (BET) method. The analysis was carried out using a Thermo Fisher Scientific S.P.A (model: Surfer Analyzer) nitrogen adsorption–desorption analyzer.

Transmission electron microscopy (TEM) (Hitachi H7100 TEM with accelerating voltage of 10 MV) was used to determine the crystal shape and the homogeneity of the catalysts.

The sample morphology was studied with Field Emission Scanning Electron Microscopy (FE-SEM) (JEOL - FE-SEM model JSM 7600F) at very high magnification by using field emission current. The sample was coated with gold to make sure of the enhance visibility of the surface and to exclusion the electrical charging of the sample during analysis.

The active site of the catalysts was evaluated by Temperature Programmed Reduction (H_2-TPR) (Thermo Finnegan TPDRO 1100) equipped with a detector of the thermal conductivity. In a reactor, about 0.05 g of catalyst was placed and treated under 150 °C for 30 min in N_2 (20 ml/min). The analysis of Hydrogen 5.51% in Argon was conducted at 50 °C and 950 °C under Argon flow (10 °C min^{-1}, 25 ml min^{-1}) and was detected by the detector of thermal conductivity.

XPS analysis was obtained using Kratos Axis Ultra DLD system, equipped with a monochromatic Al Kα (1486.6 eV), dual x-ray sources (Al & Mg), an argon etching system sample cleaning and depth profiling, parallel imaging XPS, AES, ISS and a Vision software to control the system. The base pressure of the analyzer chamber was 1×10^{-10} Torr. The excitation sources, X-ray gun was operated as a combination of 20 mA of emissions current and 15 KV

voltages. The hemispherical analyzer was run using the fixed analyzer transmission (FAT) mode for both wide and narrow scanning. This value was set at 100 eV and 40 eV of pass energy respectively. The region of interested was for the narrow scan corresponded to C1s, Mg 2p, Ce 3d, Pd 3d, and O1s photoelectron signal. The carbon charging correction refers to the binding energy of adventitious carbon at the binding energy of 285 eV. This highly sophisticated equipment is considered as a non-destructive analysis technique due to soft x-ray production to induce photoelectron emission from the sample surface. Therefore, the equipment would provide information about surface layers or thin film structures (about the top 10-100 Å of the sample).

2.3. Catalytic evaluation

The dry reforming of methane's catalytic evaluation was carried out using a fixed bed stainless steel micro-reactor (i.d. $\emptyset$ = 6 mm, h = 34 cm). The reactor was attached to a mass flow gas controller (SIERRA instrument) and an online gas chromatography (GC) (Agilent 6890N; G 1540N) equipped with Varian capillary columns HP-PLOT/Q and HP-MOLSIV. Preceding the reaction, the reduction of approximately 0.02 g catalyst took place by flowing 5% H_2/Ar (30 ml min^{-1}) at 700 ^{o}C and holding for 3 h. The reforming reaction was performed by flowing the feed which is a gas mixture composed of CH_4/CO_2 in (2/1) and (1/1) mol, at a rate of 30 ml min^{-1}. The reforming was studied from 700 to 900°C at 1 atm, then holding was carried out for 10 h (1 atm, GHSV = 15000 ml h^{-1} g^{-1}cat).

The reduction step was aimed to reduce (Pd^{+2}) phase of the palladium catalyst to Pd metal (Pd^0) phase at the active site of the catalysts. The tested catalyst was set in the middle of reactor vertically and fixed place by plugs of quartz wool. In order to control and ensure the reaction temperature, a thermocouple was placed into the catalyst chamber. The calculations of methane

10

and carbon dioxide conversions, H_2 and CO selectivity, as well as synthesis gas (H_2/CO) ratio were defined as the following equations (Eq. 7-11).

$$CH_4 \text{ Conversion } \% = \frac{CH_{4in} - CH_{4out}}{CH_{4 in}} * 100 \tag{7}$$

$$CO_2 \text{ Conversion } \% = \frac{Co_{2in} - CO_{2out}}{Co_{2 in}} * 100 \tag{8}$$

$$H_2 \text{ Selectivity } \% = \frac{H_2}{2[CH_{4in} - CH_{4out}]} * 100 \tag{9}$$

$$CO \text{ Selectivity } \% = \frac{CO}{[CH_{4in} - CH_{4out}] + [CO_{2in} - CO_{2out}]} * 100 \tag{10}$$

$$\frac{H_2}{CO} \text{ ratio } = \frac{H_2 \text{ selectivity } \%}{CO \text{ selectivity } \%} \tag{11}$$

3. Results and Discussion

3.1 Characterization of Catalysts

3.1.1 XRD patterns

Fig. 1(a,b) illustrates the XRD patterns of the reduced catalysts inclusive of magnesium and cerium. Fig. 1 was also indicated the diffraction peaks that take place at $2\theta = 37.0, 62.3, 74.7$ and $79.1°$ due to the cubic form of magnesia (JCPDS file no.: 00-002-1207). Meanwhile, the diffraction peaks at $2\theta = 28.7, 33.3, 47.8, 56.8, 59.6, 69.6, 76.8$ and 79.3 were occurred as a result of the cubic form of ceria (JCPDS file no.: 00-001-0800). However, no diffraction peaks were observed for 1% palladium in all the patterns. This may be due to the concentration of palladium was very low. This observation was in agreement with the results reported by Grange[25]. The diffraction peak of the Mg plane in XRD patterns, which was determined by the use of the Debye-Scherrer equation (Table 2), had been used to check the average crystalline size. It was found that the crystalline size was in direct proportionate with increasing amount of

ceria in the catalysts. This may be due to the effects of the remaining palladium is resting on the surface of the samples that prevents the growth of magnesia crystallites. The measurements for the sizes of the crystal were recorded as 47.3, 59.2, 60.9, and 62.3 nm for Pd/MgO, Pd/Mg$_{0.97}$Ce$^{+3}_{0.03}$O, Pd/Mg$_{0.93}$Ce$^{+3}_{0.07}$O, and Pd/Mg$_{0.85}$Ce$^{+3}_{0.15}$O, respectively. However, the sizes of the crystals; Pd/Mg$_{0.97}$Ce$^{+4}_{0.03}$O, Pd/Mg$_{0.93}$Ce$^{+4}_{0.07}$O, and Pd/Mg$_{0.85}$Ce$^{+4}_{0.15}$O were recorded as 53.6, 57.2, and 58.5 nm, respectively. The crystal system for all samples was recorded in cubic due to the cubic shaped particles inside the catalusy[26], the XRD results also supported by TEM and FESEM.

3.1.2 FT-IR Spectra

Fig. 2(a,b) shows the FT-IR data in the sample which is prepared through the impregnation of Pd(acac)$_2$ on the MgO-Ce$_2$O$_3$. The spectra of the unreduced catalysts showed bands in the region of 1800–1000 cm^{-1}, which, were characteristics of acetylacetonate ligands. The bands recorded at 1654 and 1548 cm^{-1} in the FT-IR were assigned to C=O and C=C bonds of acetylacetonate in the main catalyst (Pd(acac)$_2$) complex. Fig. 2a also shows the other bands in the spectra which showed the presence of acetylacetonate. The results were identified at 1353, 1262, 1200 cm^{-1} and the readings correspond to the C-H bond as in CH$_3$ (bending), C- C (stretching), and C- H (bending), respectively. The band at 936 cm^{-1} corresponds to C- O bond, while the peak at 671 cm^{-1} corresponds to Ce-O, as per reprted date.[27] The results for Pd(acac)$_2$/Mg$_{0.97}$Ce$^{+4}_{0.03}$O, Pd(acac)$_2$/Mg$_{0.93}$Ce$^{+4}_{0.07}$O, and Pd(acac)$_2$/Mg$_{0.85}$Ce$^{+4}_{0.15}$O, depicted the similar results as per Fig. 2b. It can be concluded that FT-IR was unable to detect the Pd-O bond because it lies at far FT-IR region. However, all the acetylacetonate peaks were disappeared after the reduction of hydrogen at a temperature of 700 $^{\circ}$C as shown in Fig. 2c.[28-29]

3.1.3 XPS analysis

XPS analysis was used to obtain information about the surface composition of unreduced catalyst Pd (acac)$_2$/Mg$_{0.85}$Ce$^{+3}_{0.15}$O. An examination of the surface of the catalyst with a few nanometer layers of 3-12 nm by XPS revealed that the emittance of photoelectron signals from C1s, Mg2p, O1s, Pd3d, Ce3d and distinguish between Ce^{3+} and Ce^{4+} as shown in Fig. 3(a-f). There were three types of carbon species as indicated by A deconvolution of a C1s narrow scan, the carbon species were identified as C-C (or C-H), C-O and C=O. The O1s photoelectron signal was produced by three types of oxygen species, namely, Mg-O, Ce-O, and Pd-O. This was also a significant split in the O1s spectrum. Two peaks were formed by the use of Mg2p (Mg-O and Mg). The peak formed by the use of Ce-O showed the highest intensity in photoelectron signal in the high binding energy region in comparison with the other peaks. Also, the narrow scan of Mg2p, Ce2p and Pd3d revealed that the composition of the oxide species of these metals, was a mixture of Mg-O, Ce-O and Pd-O respectively.[30,31]

The XPS spectra showed that the solid solution of Ce$_2$O$_3$/MgO recorded the lowest and highest binding energy of 51 and 882 eV for Mg 2p and Ce 3d, respectively. This caused the electron transfer from Ce$_2$O$_3$ to MgO, which has slowed down the reduction rate of Ce$_2$O$_3$ during the preparation of reduced catalyst. This could lead to an increase in the interaction between the two oxides, followed by the segregation of Ce atoms into tiny particles that rest on the surface of the catalyst. Consequently, there was a high dispersion of Ce, which has been accounted for the high activity of the catalyst. Following the extraction of the substrate, the segregated Ce particles interacted strongly with the remaining Ce on the substrate resulting in the attenuation of their sintering. The coke formation was prevented by the high dispersion of Ce, which required large Ce clusters. The TEM analysis revealed that the Ce$_2$O$_3$–MgO solid solution which was highly

effective consists of crystallite sizes of about 80 nm. The solid solution was unchanged throughout the 50 h of reaction at 900°C.[32]

In this study, XPS was used for the analysis of the compound $Pd/Mg_{0.85}Ce^{+4}_{0.15}O$. It was noted that there was differences between the peaks of Ce3d of $Pd/Mg_{0.85}Ce^{+4}_{0.15}O$ and Ce3d of $Pd/Mg_{0.85}Ce^{+3}_{0.15}O$. As per Fig. 3 (f) Ce(III) and Ce(IV) spectra have different multiplet splitting, so, Ce(IV) showed peak at 917eV which was absent in Ce(III) spectrum. The concentration of Ce^{3+} was observed high as compred to Ce^{4+} due to which Ce^{3+} showed more activity and stability as well.

3.1.4 TEM and FE-SEM

Fig. 4(a-g) illustrates the distribution, morphology and size of the synthesized catalysts. The smallest crystals, approximately 50–80 nm, were characterized by TEM through the analysis of cubic structure and crystal sizes. Fig. 5(a-g) shows the morphology of the catalyst that was supported by the analysis of FE-SEM. It was found that the regular shaped particles support $Pd/Mg_{0.97}Ce^{3+}_{0.03}O$, $Pd/Mg_{0.93}Ce^{3+}_{0.07}O$, $Pd/Mg_{0.85}Ce^{3+}_{0.15}O$ catalysts.[33] Meanwhile, the crystal Pd particles was uniformly supported the regular shaped supports which forms a smaller particle size of Pd and a greater homogeneity in metal dispersion. Fig. 4(a-g) illustrates a two-dimensional cubic texture was devoted to the catalyst.[34] The pores of the catalyst were of uniform size ~18 nm, which, was also consistent with the BET results as presented in Table 2. Some of the Pd particles were uniformly loaded on the external surface of the $Mg_{0.85}Ce_{0.15}O$ support, which varies considerably from the crystalline sites inside the porous structure. The difference in the sizes of Pd particles may be due to the growth of regulated crystals inside the narrowly distributed channels, thus causing less homogeneity of Pd particles in comparison to the other catalysts. It was found that the particle size of the supported Pd showed an increase in

the following sequence; $Pd/Mg_{0.85}Ce^{3+}_{0.15}O < Pd/Mg_{0.93}Ce^{3+}_{0.07}O < Pd/Mg_{0.97}Ce^{3+}_{0.03}O$, which corresponds to the equation results of Scherrer.

3.1.5 Surface area and porosity of the catalyst

Table 2 presents the value of the specific surface area of BET (S_{BET}) and the pore properties of reduced catalyst supports. The Pd/ MgO catalyst had a pore radius of 11.4 ^{o}A, a pore volume of 0.2122 cm^3/g, and a surface area of 15.7 m^2/g. However, the addition of Ce_2O_3 as a promoter had caused a reduction in the surface area and volume as well. This decrease may be due to strong interaction between palladium and magnesia-ceria support, and also due to pore blocking during the impregnation process. The observation of the present study were agreed with earlier reports.[35] However, the addition of Ce_2O_3 had prevented the loss of surface area during calcinations at a temperature of 1150 ^{o}C, which were resulted in the elevation of the surface area of the catalyst (Table 2). The following surface areas 6.3, 7.5, and 16.6 m^2/g were for Pd/ $Mg_{0.97}Ce^{3+}_{0.03}$, Pd/ $Mg_{0.93}Ce^{3+}_{0.07}O$ and Pd/ $Mg_{0.85}Ce^{3+}_{0.15}O$, respectively, while the 8.1, 9.3, and 9.8 m^2/g, corresponds to Pd/$Mg_{0.97}Ce^{4+}_{0.03}$, Pd/ $Mg_{0.93}Ce^{4+}_{0.07}O$ and Pd/ $Mg_{0.85}Ce^{4+}_{0.15}O$, respectively.

It was obsereved that when the size of cerium increases, the surface area also showed an increase. The pore radius of all the catalysts were affected by the concentration level of the Ce_2O_3. The following pore radis of Ce_2O_3 at 23.6, 24.3, and 90.1^{o}A for Pd/$Mg_{0.97}Ce^{3+}_{0.03}O$, Pd/$Mg_{0.93}Ce^{3+}_{0.07}O$ and Pd/$Mg_{0.85}Ce^{3+}_{0.015}O$, respectively, whereas, the recording of Ce_2O_3 at 23.3, 25.6, 30.9 ^{o}A corresponds to Pd/$Mg_{0.97}Ce^{4+}_{0.03}O$, Pd/$Mg_{0.93}Ce^{4+}_{0.07}O$ and Pd/$Mg_{0.85}Ce^{4+}_{0.015}O$, respectively. After the addition of cerium, the pore volume was increased slightly i.e. 0.0946, 0.1055, 0.123 cm^3/g for Pd/$Mg_{0.97}Ce^{3+}_{0.03}O$, Pd/$Mg_{0.93}Ce^{3+}_{0.07}O$ and

15

Pd/Mg$_{0.85}$Ce^{3+}$_{0.015}$O, respectively. The findings showed that there is no apparent relation between the S$_{BET}$ value and the pore volume of the catalysts.[36]

3.1.6 Temperature programmed reduction (TPR)

TPR-H$_2$ was used to characterize the reducibility of cerium for the reforming of Pd catalysts. Fig. 6a and Table 3 tabulates the profiles of TPR-H$_2$ for Pd/Mg$_{1-x}$Ce^{+3}$_x$O (where x= 0.00, 0.03, 0.07, 0.15) as well as illustrated in the TPR-H$_2$ patterns of the catalysts. Pd/MgO catalyst showed a peak which was formed when the temperature recorded at 247 °C, this may be due to the reduction in Pd-O crystallite.[37] Fig. 6a shows the profile of TPR-H$_2$ for Pd/Mg$_{0.97}$Ce^{+3}$_{0.03}$O, Pd/Mg$_{0.93}$Ce^{+3}$_{0.07}$O, and Pd/Mg$_{0.85}$Ce^{+3}$_{0.15}$O of a cubic structure with three peaks. The first peak was formed when the temperatures recorded 215°C, 213°C and 232°C, for Pd/Mg$_{0.97}$Ce^{+3}$_{0.03}$O, Pd/Mg$_{0.93}$Ce^{+3}$_{0.07}$O, and Pd/Mg$_{0.85}$Ce^{+3}$_{0.15}$O, respectively, due to the reduction of Pd-O to Pd^0. The second peak was formed when the temperatures recorded 494°C, 503°C and 508 °C, for Pd/Mg$_{0.97}$Ce^{+3}$_{0.03}$O, Pd/Mg$_{0.93}$Ce^{+3}$_{0.07}$O, and Pd/Mg$_{0.85}$Ce^{+3}$_{0.15}$O, respectively, This corresponds to the reduction in the surface area of Ce$_2$O$_3$ in the catalysts Pd/Mg$_{1-x}$Ce^{+3}$_x$O. Meanwhile, the third peak was formed when the temperature recorded 749°C, 754°C and 764 °C for Pd/Mg$_{0.97}$Ce^{+3}$_{0.03}$O, Pd/Mg$_{0.93}$Ce^{+3}$_{0.07}$O, and Pd/Mg$_{0.85}$Ce^{+3}$_{0.15}$O, respectively, which is in relation to the bulk reduction of CeO$_2$. The second peak was reduced at lower temperatures due to the lower enthalpy of reduction, followed by a bulk reduction at higher temperatures. The first possible reason for this could be an improved dispersion of Ce$_2$O$_3$ particles due to the incorporation of MgO into Ce$_2$O$_3$ and retardation of sintering.[38] The other possible reason could be a stronger interaction between CeO$_2$ and Pd. The overlapping of the PdO and reduction of the CeO$_2$ peaks may have contributed to the strong interaction.[39] It was resulted in the dispersion of a good promoter to the support and a high interaction with Pd species. It is deduced that the H$_2$-

consumption of 224.6 µmol/g catalyst was used for the reduction of total Pd-O to Pd on Pd/MgO. The total amount of H_2-consumption of the reduced $Pd/Mg_{0.97}Ce^{+3}_{0.03}O$, $Pd/Mg_{0.93}Ce^{+3}_{0.07}O$, and $Pd/Mg_{0.85}Ce^{+3}_{0.15}O$ was calculated from the area of the three peaks. The findings of the catalysts were recorded as 312.5, 414.9, and 561.1 µmol/g, respectively. This may be indicates a reduction of Pd-O, and partial reduction of Ce_2O_3. The addition of the promoter Ce_2O_3 increases the reducibility of catalysts, especially for catalysts with MgO support. This may be due to the acidic-basic properties of the support. It is clear that $Mg_{1-x}Ce^{+3}_xO$ with the higher basicity than MgO interact strongly with Ce_2O_3 promoter and resulted in better Pd-O reduction with respect of the redox property of $Mg_{1-x}Ce^{+3}_xO$.[36,40]

Meanwhile, Fig. 6b and Table 3 illustrates the TPR-H_2 profiles of $Pd/Mg_{0.97}Ce^{+4}_{0.03}O$, $Pd/Mg_{0.93}Ce^{+4}_{0.07}O$, and $Pd/Mg_{0.85}Ce^{+4}_{0.15}O$. The TPR-$H_2$ patterns of these catalysts were also similar to that of the previous catalysts. For all the three catalysts, it was detected that each catalyst had three distinct peaks. The temperatures recorded at the first peak were 210 °C, 217 °C and 233 °C, which, was attributed to the reduction of Pd-O to Pd^0. The temperatures recorded at the second peak were 498 °C, 505 °C and 513 °C. This was attributed to the reduction of CeO_2 on the surface. Finally, the temperature recorded at the final peak were 744 °C, 760 °C and 776 °C, which, was attributed to the reduction of bulk CeO_2 for $Pd/Mg_{0.97}Ce^{+4}_{0.03}O$, $Pd/Mg_{0.93}Ce^{+4}_{0.07}O$, and $Pd/Mg_{0.85}Ce^{+4}_{0.15}O$, respectively. The best explanation for the high reduction in temperature of $Pd/Mg_{1-x}Ce^{+4}_xO$ as compared to $Pd/Mg_{1-x}Ce^{+3}_xO$ may be the emergence of overlapping peaks after the reduction of PdO and CeO_2.[41] As the Ce^{+3} ion is less charged and bigger in size than the Ce^{+4} ion, it is easier for the reduction of Ce^{+3}. Based on the area of the two peaks, the H_2-consumption of $Pd/Mg_{0.97}Ce^{+4}_{0.03}O$, $Pd/Mg_{0.93}Ce^{+4}_{0.07}O$, and $Pd/Mg_{0.85}Ce^{+4}_{0.15}O$ reduction was recorded at 267.8, 388.9 and 456.5 µmol/g catalyst, respectively. The TPR-H_2 results reveal that

17

the $Pd/Mg_{0.85}Ce^{+3}_{0.15}O$ catalyst were showed the highest active sites among the other catalysts. Thus, it can be concluded that $Pd/Mg_{0.85}Ce^{+3}_{0.15}O$ was the best catalyst in the present study.

3.1.7 Thermal analysis study

Fig. 7a shows the TGA analysis for the reduced catalysts: Pd/MgO, $Pd/Mg_{0.97}Ce^{+3}_{0.03}O$, $Pd/Mg_{0.93}Ce^{+3}_{0.07}O$, and $Pd/Mg_{0.85}Ce^{+3}_{0.15}O$. The results revealed that there was weight loss at only one stage for all the catalysts. The estimated weight loss was approximately 2%, which, occured at a temperature between 100 °C and 150 °C. This can be attributed to the removal of moisture from the $Pd/Mg_{1-x}Ce_xO$ catalysts, as shown in Fig. 7a. In contrast, the estimated weight loss for Pd/MgO, $Pd/Mg_{0.97}Ce^{+3}_{0.03}O$, $Pd/Mg_{0.93}Ce^{+3}_{0.07}O$, and $Pd/Mg_{0.85}Ce^{+3}_{0.15}O$ catalysts was recorded at 1.5%, 2.2%, 1.8% and 1.6%, respectively. Meanwhile, the estimated weight loss for $Pd/Mg_{0.97}Ce^{+4}_{0.03}O$, $Pd/Mg_{0.93}Ce^{+4}_{0.07}O$, and $Pd/Mg_{0.85}Ce^{+4}_{0.15}O$ catalysts was recorded at 2.0%, 1.7% and 1.6%, respectively. The graphs below showed the whole weight of the compound. There was a slight increase at first due to the adsorption of the N_2 gas on the compound. All the compounds became thermally stable at 500°C, which corresponds to the high melting point of Magnesia and Ceria at 2852°C, 2177 °C, respectively. It also helps in establishing good interaction among the components of the catalyst. Fig.7b was illustrated the components of the other catalysts: $Pd/Mg_{0.97}Ce^{+4}_{0.03}O$, $Pd/Mg_{0.93}Ce^{+4}_{0.07}O$, and $Pd/Mg_{0.85}Ce^{+4}_{0.15}O$. The findings of the thermal analysis were similar and consistent with the results of Mojovic et al.[42]

3.2 Catalytic Performance in biogas reforming

3.2.1 Effect of reactant concentration on conversion

The conversion of CH_4 and CO_2, and the selectivity, which is defined in terms of the H_2/CO ratio showed the dry reforming reaction activity. When the temperature increases over than 900°C,

blank tests (reaction without catalyst) showed the existence of H_2 and CO in the outlet gas. This may be due to methane decomposition reaction (Eq. 4). When $Mg_{1-x}Ce_xO$ was used without Pd, the conversion of CH_4 and CO_2 were recorded at low reading of 38% and 48%, respectively, while the H_2/CO ratio recorded 0.2%. These results indicated that there may be a weak reaction on the promoter pores of the support, which was presented in the BET results. On the other hand, when the catalyst $Pd/Mg_{1-x}Ce^{3+}_xO$ were used, the rate of conversion of CH_4 and CO_2 and the H_2/CO ratio showed an increase. Figure.8 illustrated the effects of the reactant ratio on the H_2/CO ratio and CO_2 conversion. The concentration of CO_2 (CH_4:CO_2, 1:1), was increased, which, followed by an increase in the conversion of CO_2 as well as the ratio of H_2/CO. This occurrence could be due to the decrease in the carbon deposition on the surface of the catalyst that reacted with excess CO_2 to produce CO (Eq. 6) . In other words the doped Pd metal on the support plays a crucial role in the catalytic reaction. It had been observed that $Pd/Mg_{0.85}Ce_{0.15}O$ catalyst recorded a conversion of 54% and 74% for CH_4:CO_2 (1:1), and a H_2/CO ratio of 0.6. However, the conversion of the gases, CH_4 and CO_2 was recorded at 58% and 45%, respectively, as the ratio of (2:1) and the H_2/CO ratio was 0.3. This finding indicated that the best resistance to the deactivation of the catalyst stands at the ratio of 1:1 due to carbon formation which helped in the formation of high selectivity of H_2 and CO (Fig. 8). The same results were also obtained from the other reported catalysts.[43]

3.2.2 Effect of catalyst concentration on conversion

Fig. 9 and Table 4 illustrate the effects of the concentration of catalysts on the conversion process. It had shown that the values of CH_4 and CO_2 conversion and H_2/CO ratio was 45%, 66% and 0.3 for Pd/MgO catalyst, whereas $Pd/Mg_{0.97}Ce^{3+}_{0.03}O$ catalyst showed 49%, 67% and 0.5, and for $Pd/Mg_{0.93}Ce^{3+}_{0.07}O$ catalyst, the values were at 46%, 66% and 0.4. The highest

19

values for Pd/ $Mg_{0.85}Ce^{3+}_{0.15}O$ catalyst were reported as 54%, 74% and 0.6 for the CH_4 and CO_2 conversion and H_2/CO ratio.

In this study, the results were favorable may be due to good interaction between Pd metal and support as well as a good basicity of the support. In previous studies, Laosiripojana[44] and Guo et al.[45] showed unfavorable results. This was because the researchers used the catalyst Ni/Al_2O_3, which had weak interaction between Ni and the support Al_2O_3, also the catalyst had produced low basicity of alumina.

The increasing order of CH_4 and CO_2 conversion and the H_2/CO ratio can be described as Pd/MgO < Pd/$Mg_{0.97}Ce^{3+}_{0.03}O$ < Pd/$Mg_{0.93}Ce^{3+}_{0.07}O$ < Pd/ $Mg_{0.85}Ce^{3+}_{0.15}O$. This means that the best catalyst was Pd/$Mg_{0.85}Ce_{0.15}O$. The results indicated that the rate of the formation of CO in the dry reforming of methane depends on the amount of Ce_2O_3–MgO solid solution in the catalyst.[46] It might be concluded that the greater amount of solid solution, the higher is the rate of formation of CO. Hence, the formation of a solid solution plays an important role in the generation of the active sites for the CO_2 reformation of methane. This occurs because the entire Ce_2O_3 is like a solid solution, which stabilizes both oxides. Only the surface layer of Ce_2O_3 of the catalyst of the solid solution, Ce_2O_3–MgO was reduced to 700^oC. The Ce sites that were generated remained in close contact with the solid solution which hindered the Ce sintering.[46] In addition the activity of the catalyst, Pd/$Mg_{0.85}Ce^{3+}_{0.15}O$ was more than the activity of the catalyst Pd/$Mg_{0.85}Ce^{4+}_{0.15}O$. This may be due to the charge of Ce^{3+} is lesser than the charge of Ce^{4+}. In this way, reduction is easier, while Ce is produced on the surface of the catalyst.

Furthermore, Pd particles can be found in the sites responsible for the catalytic process because Pd particles have strong interaction with MgO-Ce_2O_3. It is also noted that increasing the

Pd concentration in the support had not changed the CH_4 conversion and CO_2 conversion and selectivity. This can be attributed to the formation of strong Lewis basicity with a metal oxide support. An increase in the Lewis basicity of the support, has subsequently increased the ability of the catalyst in the dry reforming of methane for the chemisorb of CO_2. Besides, the adsorbed CO_2 will react with C to form CO (Eq. 6), which leads to a reduction in the coke formation. The formation of the solid solution Ce_2O_3–MgO also provides a specific approach to suppress the deposition of carbon. MgO is linked to a strong Lewis base, with a high amount of CO_2 on the surface of the catalyst that can decrease or prevent carbon formation. Furthermore, the XPS results, showed that the reduction of Ce_2O_3 was much more difficult for the Ce_2O_3–MgO solid solution than the solid solution of pure Ce_2O_3. The reduction may leads to the formation of small particles of cerium on the surface.[47,48] The combination of the surface basicity and the small metal particle size (Table 2) affects the carbon deposition by the MgO-based solid solution catalysts.

Furthermore, the high conversion rate of CH_4 and CO_2 was due to the particle size involved in the reaction activity. The doping metal Pd was prepared based on the Debye Sherrer equation, and supported by TEM analysis. Its particle size was as tiny as nanoparticles. Thus, it is evident that particle size plays a significant role in the reaction activity. Any increase in the conversion of reactants and the selectivity (yield) can be attributed to the reduction of particles into nano-ranged sizes, which can lead to an increase of 16.6 m^2/g in the surface area and 561.1 µmol/g of active sites (Table. 2).

3.2.3 Effects of temperature on conversion

Fig. 10 shows the activity and selectivity results of the catalyst Pd/ $Mg_{0.85}Ce_{0.15}O$ at a range of temperature from 700 to 900°C. In general, the conversion of CH_4:CO_2 (1:1) showed an increase

when the temperature was raised from 700°C to 900°C. This may be due to the strong endothermic reaction reaction of dry-reforming (Eq. 2). Earlier studies had shown that higher temperature increased the rate of conversion.[49] It is noted that when there was an increase in temperature from 700°C to 900°C, the CH_4 conversion of $Pd/Mg_{0.85}Ce_{0.15}O$ showed an increase from 48% to 54% and the CO_2 conversion also marks an increase from 18% to 74%. However, when the temperature was above 900°C, there was no evident increase in conversion rates of CH_4 and CO_2. Fig. 10 showed the H_2/CO ratio of the catalyst at different temperatures. When the temperature was below 900°C, the H_2/CO ratio of the samples was recorded at <1. The reverse water-gas-shift reaction (RWGS), (Eq. 2) might consume the extra H_2 and produce CO, which causes a fall in the H_2/CO ratio. When the temperature was at 900°C, the H_2/CO ratio of $Pd/Mg_{0.85}Cei_{0.15}O$ was recorded at 0.6, which indicates that small contribution from the RWGS reaction (Eq. 3).[50] Table 3 shows that the activity and selectivity of $Pd/Mg_{1-x}Ce^{3+}_{x}O$ was higher than that of $Pd/Mg_{1-x}Ce^{4+}_{x}O$ in DRM. This might be due to Ce(III)-based catalysts are better than Ce(IV)-based catalysts in terms of lower charge, bigger Ce^{3+} ion, and easier reduction to Ce.[51]

3.2.4 Stability tests

Fig. 11 shows the findings of the temperature tests. It is revealed that at 900°C, the conversions for both CH_4 and CO_2 were high. In general, CH_4 is only adsorbed on the palladium metal and dissociated to yield of hydrogen and hydrocarbon species CH_x (x=0-4), IF x=0. The deposition of carbon on the surface of Pd metal[52] is elaborated through the following mechanisms:

$$CH_4 + 2Pd_{(as)} \longrightarrow CH_3Pd_{(as)} + HPd_{(as)}$$

$$CH_3Pd_{(as)} + Pd_{(as)} \longrightarrow CH_2Pd_{(as)} + HPd_{(as)}$$

$$CH_2Pd_{(as)} + Pd_{(as)} \longrightarrow CHPd_{(as)} + HPd_{(as)}$$

$$CHPd_{(as)} + Pd_{(as)} \longrightarrow CPd_{(as)} + HPd_{(as)}$$
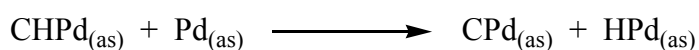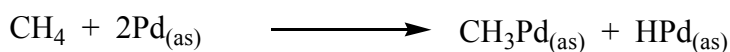
$$2HPd_{(as)} \longrightarrow H_{2(g)} + 2Pd_{(as)} \qquad \text{(as) metal active site}$$

22

Nakamura et al.[53] had investigated the effects of the catalyst promoter on dry reforming of methane. According to the mechanisms, CO_2 was activated in proximity to the metal particle on the support to form a carbonate species. Finally, carbonate was reduced by CH_x species to form carbon monoxide (CO).

.

$$CO_{2(g)} \longrightarrow CO_{2(support)}$$

$$CO_{2(support)} + O^{2-}_{(support)} \longrightarrow CO_3^{-2}_{(support)}$$

$$2H_{(metal)} \longrightarrow 2H_{(support)}$$

$$CO_3^{-2}_{(support)} + 2H_{(support)} \longrightarrow HCO_2^{-1}_{(support)} + OH^{1-}_{(support)}$$

$$CO_{(support)} \longrightarrow CO_{(g)}$$
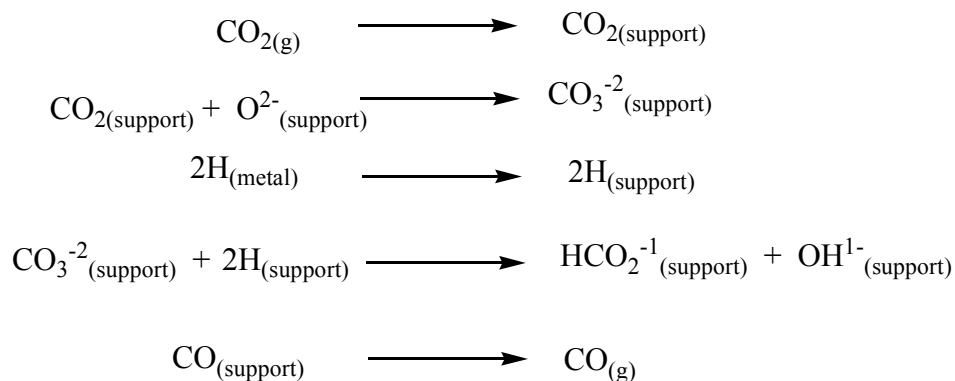
The function of the promoter Ce_2O_3 in the catalyst is to produce high stability and resistance against coking. This is confirmed by the results obtained from the conversion of CO_2 and CH_4 as well as a H_2/CO ratio for over 50 h of reaction. The formation of carbon on the palladium surface of the catalyst in the dry reforming of methane was eliminated by Ce_2O_3. While the CO_2 adsorption was enhanced by increasing the basicity of Ce_2O_3, the formation of carbonate species occurs mainly on Ce_2O_3, which was dissociated into CO_2, which is then dissociated into CO and O. The oxygen then reacts with the carbon deposited on the Pd metal to produce CO.[54] When the concentrations of Ce_2O_3 were low, the CO_2 conversion increased through the formation of strong ionic oxides $Ce_2O_2CO_3$, which resulted in the adsorption of CO_2 on the surface of the catalyst, This reaction was elevated the conversion of CH_4. When Ce_2O_3 was found in higher concentrations, the conversion of both CH_4 and CO_2 attenuated. This may be most likely due to the increase in the electron density of Pd.[55] The $Ce_2O_2CO_3$ species participate directly in DRM, where, it decompose to produce CO and this provides the oxygen species to react with the carbon deposits at the interface of $Pd-Ce_2O_2CO_3$. Following this activity, the Pd

sites were restored in the process. Likewise, Ce_2O_3 had supported the catalysts to dissociate in adsorbed CO_2.

$$CO_{2(g)} \longrightarrow CO_{(support)} + O_{(promoter)}$$

$$C_{(metal)} + O_{(promoter)} \longrightarrow CO_{2(g)}$$
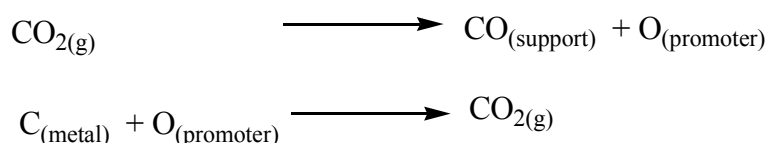
Fig.13 illustrates the thermo-grams in two different temperature regions. At the first stage of the temperature range, there was a decrease in weight of the spent catalyst. On the contrary, there was an increase in weight at a higher temperature. When the temperature was at 650°C, the weight loss was attributed to the oxidation of the carbon deposit. The carbon deposited on the spent catalyst was considered to be carbon layered. Further layering of carbon was found in the absence of filamentous carbon, as indicated in the TEM results of spending catalysts (refer to Fig. 12). The amount of coke deposited on spent catalyst was calculated to be 1% wt. In conclusion, the results showed that a little amount of coke was deposited on the catalysts, and the formation of coke was likely due to metal dispersion of the catalysts. The smaller crystal size of metal catalysts makes a catalyst less prone to deactivation. This finding was in line with the reported results by Zhu et al.[56]

4. Conclusions

Co-precipitation method was used to prepare samples of $Pd/Mg_{1-x}Ce^{3+}_xO$ and $Pd/Mg_{1-x}Ce^{4+}_xO$ (x = 0.00, 0.03, 0.07, and 0.15) (with 1% wt Pd loading) with K_2CO_3 as a precipitant. These samples were used as catalysts for the syngas synthesis after the reaction of CO_2 reforming of methane under ideal reaction conditions by T = 900°C, and CH_4/CO_2 = 1/1, with catalyst, $Pd/Mg_{0.85}Ce^{3+}_{0.15}O$. The results of the XRD analysis maintained that traces of Ce_2O_3 were found in the MgO lattices and also on the surfaces of the catalysts. The findings also revealed that some photoelectron signals were emitted from C1s, Mg2p, O1s, Pd3d, and Ce3d. The results of TPR

24

showed that the reducibility of Ce_2O_3 was increased by an increase in Ce_2O_3 in the support with high active sites on the catalyst's surface. For dry reforming of methane, the CO_2 and CH_4 conversion recorded 74%, 54 %, respectively, for the catalyst, $Pd/Mg_{1-x}Ce^{3+}_x O$. This result was higher than the catalyst, $Pd/Mg_{1-x}Ce^{4+}_x O$ at 900^oC. In addition, the CO_2 and CH_4 conversion for the catalyst, $Pd/Mg_{1-x}Ce^{4+}_x O$ was found to be lower than that for the catalyst $Pd/Mg_{1-x}Ce^{3+}_x O$ due to smaller size of Ce^{4+} ion. Finally, a positive charge ion can cause a weaker reducibility than a Ce^{3+} ion in the catalyst.

Acknowledgements

Notes and references

1 D. C. Carvalho, H. S. Souza, M. Josué Filho, E. M. Assaf, V. V. Thyssen, A. Campos, and A. C. Oliveira, *RSC Adv.*, 2014, **4**, 61771-61780.

2 A. R. McFarlane, I. P. Silverwood, R. Warringham, E. L. Norris, R. M. Ormerod, C. D. Frost, and D. Lennon, *RSC Adv.,* 2013, **3**, 16577-16589.

3 R. G. Gonzalez, *Petrol. Tech. Q.* 2006, **11**, 61–62.

4 J. G. Zhang, H. Wang and K. D. Ajay, *J. Catal.* 2007, **249**, 300–310.

5 Z. L. Zhang and X.E. Verykios, *Catal. Today.*, 1994, **21**, 589-595.

6 E. Ruckenstein and Y.H. Hu, *Adv. Catal.* 2004, **48**, 297-345.

7 H.B. Nussler and O. Z. Kubaschewski, *Phys. Chem.* 1980, **121**, 187-195.

8 V. M. Shinde, and G. Madras, *RSC Adv.,* 2014, **4**, 4817-4826.

9 J. T. Richardson, M. Garrait and J. K. Hung, *Appl. Catal. A.,* 2003, **255**, 69–82.

10 K. Seshan, H. W. Ten Barge, W. Halty, A. N. J. Van Keulen and J. R. H. Ross, *Stud. Surf. Sci. Catal.* 1994, **81**, 285–290.

11 K. Tao, S. Zhou, Q. Zhang, C. Kong, Q. Ma, N. Tsubaki and L. Chen, *RSC Adv.,* 2013, **3**, 22285-22294.

12 J. A. C. Dias, J. M. Assaf, *Catal. Today* 2003, **85**, 59–68.

13 J. Juan-Juan, M. C. Romn-Martnez and M. J. Illn-Gmez, *Appl. Catal. A.,* 2006, **301**, 9–15.

14 A. E. C. Luna and M. E. Iriarte, *Appl. Catal. A.,* 2008, **343**, 10–15.

15 K. C. Mondal, V. R. Choudhary and U. A. Joshi, *Appl. Catal. A* 2007, **316**, 47-52.

[16] D. Dong, X. Shao, Z. Wang, C. Lievens, J. Yao, H., Wang and C. Z. Li, *RSC Adv.*, 2013, **3**, 1341-1345.

17 Q. Zhang, T. Wu, P. Zhang, R. Qi, R. Huang, X. Song and L. Gao, *RSC Adv.*, 2014, **4**, 51184-51193.

18 H. Kambolis, A. Matralis, C. Trovarelli, C.H. Papadopoulou, *Appl. Catal. A: Gen.* 2010, **377**, 16-26.

19 J. L. G. Fierro, J. Soria, J. Sanz and J. M. Rojo, *J. Solid State Chem.* 1987, **66**, 154-162.

20 A. Trovarelli, *Catal. Rev-Sci. Eng.* 1996, **38**, 439-520.

21 S. Damyanova, B. Pawelec, K. Arishtirova, M.V. Martinez-Huerta and J.L.G. Fierro, *Appl. Catal. B: Environ.* 2009, **89**, 149-159.

22 J. Chen, Q. Wu, J. Zhang and J. Zhang, *Fuel*, 2008, **87**, 2901-2907.

23 K. Tomishige, *Catal. Today*, 2004, **89**, 405-418.

24 F. W. Aldbea, N. Ibrahim, M. H. Abdullah and R. E Shaiboub, *J. Sol-gel Sci. Technol.* 2012, **62**, 483-489.

25 P. Grange, *Catal Rev-Sci. Eng.,* 1980, **21**,135-181.

26 X. Wang, L. Meng, F. Wu, L. Wang and X. Mu, *J. Green Chem.* 2012, **14**, 758-767.

27 S.A. Sadeek, *J. Argentine Chem Soc.,* 2005, **93**, 165-175.

28 K. Walter, O. Seiferth, J. Libuda, H. Kuhlenbeck, M. Ba¨umer and H.-J. Freund, *Surf. Sci.,* 1998, **402**, 428–432.

29 F. Skoda, M. P. Astier, G. M. Pajonk and M. Primet, *Catal. Lett.* 1994, **29**, 159-168

30 M. Zhiijian, L. Ying, F. Maohong, Z. Ling, Z. Ji, *J. Chem. Eng.* 2015, **259**, 293-302.

31 C. Hidalgo, S. Jalila, M. Alberto, M. Jose and S. Said, *J. Colloid Inter. Sci.* 2012, **382**, 67-73.

32 E. Ruckenstein and Y.H. Hu, *Chem. Inno.,* 2000, **30**, 39-43.

33 X. Chen, J. Jiang, F. Yan, S. Tian and K. Li, *RSC Adv.,* 2014, **4**, 8703-8710.

34 L. Qian, Z. Ma, Y. Ren, H. Shi, B. Yue, S. Feng, J. Shen and S. Xie, *Fuel*, 2014, **122**, 47-61.

35 B. Saha, A. Khan, H. Ibrahim and R. Idem, *Fuel*, 2014, **120**, 202-217.

36 Y. H. Taufiq-Yap, Sudarno, U. Rashid, Z. Zainal, *Appl. Catal. A-Gen.*, 2013, **468**, 359-369.

37 G. Li, L. Hu and M. Hill, *Appl. Catal. A Gen.* 2006, **301**, 16–24.

38 M. Fernandez-Garcia, A. Martiner-Arias and A. IglesiasJuez, *J. Catal.* 2000, **194**, 385-392.

39 Y. W. Chao and P. K. Shen *Inter. J. Hydro. Energ.,* 2012, **37**, 4107-4118.

40 S. Tada, T Shimizu, H Kameyama and T Haneda, *Inter. J. Hydro. Energ.,* 2012, **37**, 5527-5531.

41 V.M. Gonzalez-Delacruz, F. Ternero, R. Peren, A. Caballero and J.P. Holgado. *Appl Catal A Gen.*, 2010, **384**, 1-9.

42 Z. Mojovic, S. Mentus and Z. Tesic, *Mater. Sci. Forum*, 2004, **453**, 257-263.

43 A. M. Gadalla and M. E. Sommer, *Chem. Eng. Sci.* 1989, **44**, 2825-2829.

44 N. Laosiripojana and S. Assabumrungrat, *Appl. Catal. B: Environ.* 2005, **60**, 107–116.

45 J. Guo, H. Lou, H. Zhao, D. Chai, X. Zheng, *Appl. Catal. A Gen.* 2004, **273**, 75–82.

46 A. Zecchina, G. Spoto and S. Coluccia, J. Chem. Soc., *Faraday Trans. I.*, 1984, **80**, 1891-1901.

47 Y. H. Hu and E. Ruckenstein, *Catal. Rev.* 2002, **44**, 423-453.

48 K. Tomishige, Y. Himeno, Y. Matsuo, Y. Yoshinaga and K. Fujimoto, *Ind. Eng. Chem. Res.* 2000, **39**, 1891-2021.

49 S. Appari, V. M. Janardhanan, R. Bauri, S. Jayanti, Deutschmann, O., *Appl. Catal. A-Gen.* 2014, **471**, 118-125.

50 J. Kehres and Jakobsen, *J. Phys. Chem. C*, 2012, **116**, 12407-21415.

51 D.L. Trimm, *Catal. Today* 1997, **37**, 233–238.

52 A. Topalidis, D. E. Petrakis, A. Ladavos, L. Loakatzikou and P. J. Pomonis, *Catal. Today*, 2007, **127**, 238-245.

53 J. Nakamura, K. Aikawa, K. Sato and T. Uchijima, *Catal. Lett.* 1994, **25**, 265-270.

54 T. Osaki and T. Mori, *J. Catal.* 2001, **204**, 89-97.

55 J. A. C. Dias and J. M. Assaf, *Catal. Today*, 2003, **85**, 59-68.

56 J. Zhu, X. Peng, L. Yao, J. Shen, D. Tong and C. Hu, *Int. J. Hydro. Energ.* 2011, **36**, 7094-7104.

28
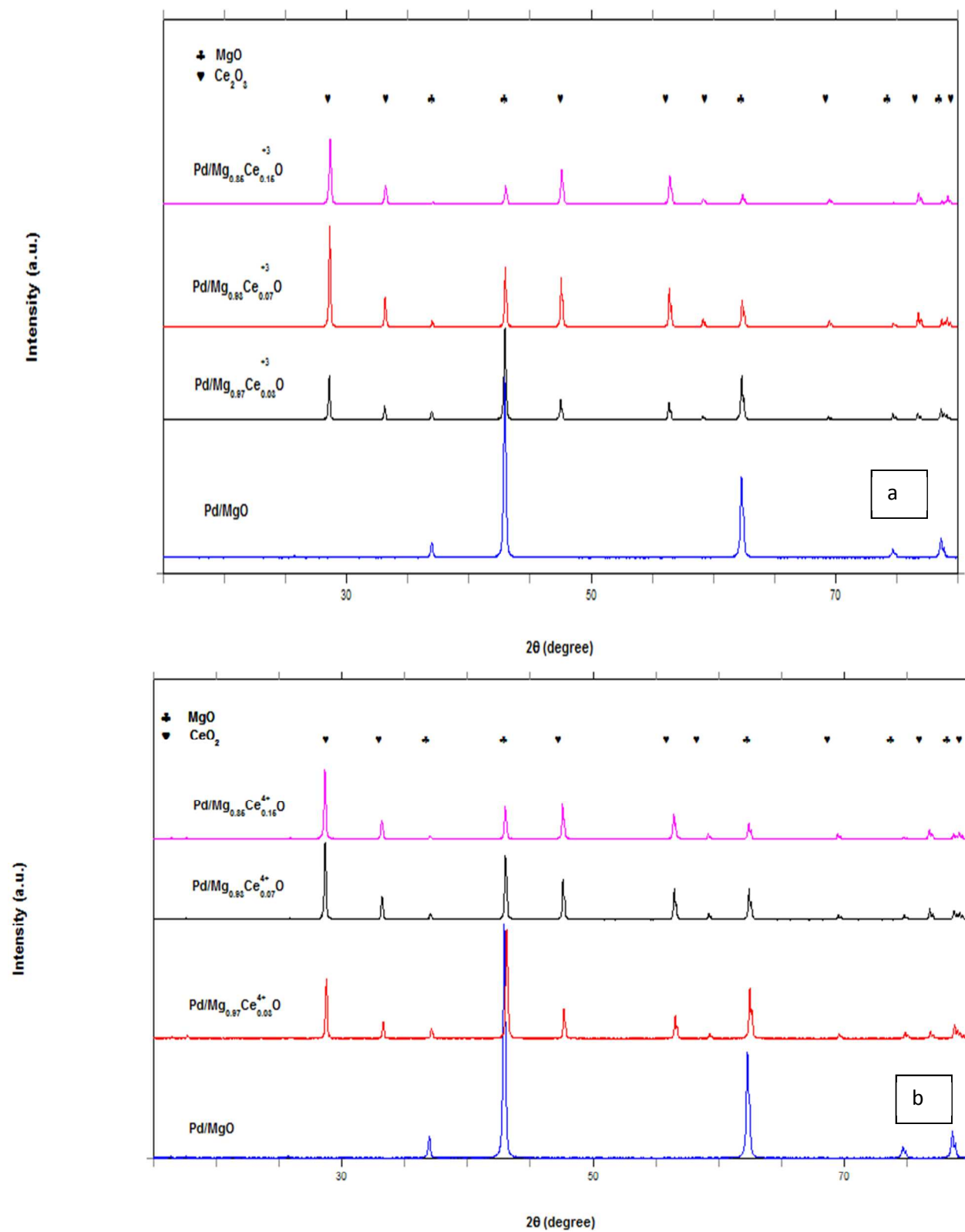
Fig. 1 XRD patterns of the catalysts with (a) Ce^{3+} and (b) Ce^{4+} promoter.

29

$Pd(acac)_2/Mg_{0.85}Ce^{3+}_{0.15}O$

$Pd(acac)_2/Mg_{0.93}Ce^{3+}_{0.07}O$

$Pd(acac)_2/Mg_{0.97}Ce^{3+}_{0.03}O$

$Pd/(acac)_2MgO$

(a)

Transmittance %

W a v e   n o . (C m^{-1})

$Pd(acac)_2/Mg_{0.85}Ce^{+4}_{0.15}O$

$Pd(acac)_2/Mg_{0.93}Ce^{+4}_{0.07}O$

$Pd(acac)_2/Mg_{0.97}Ce^{+4}_{0.03}O$

$Pd(acac)_2/MgO$

(b)

Transmittance %

W a v e   n o . (C m^{-1})

30
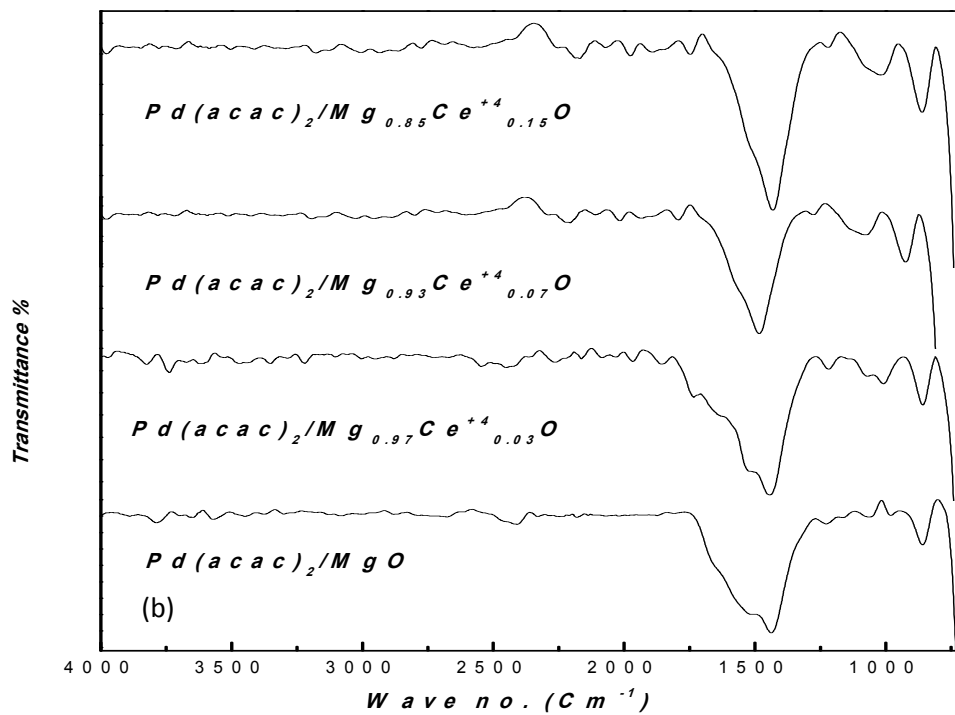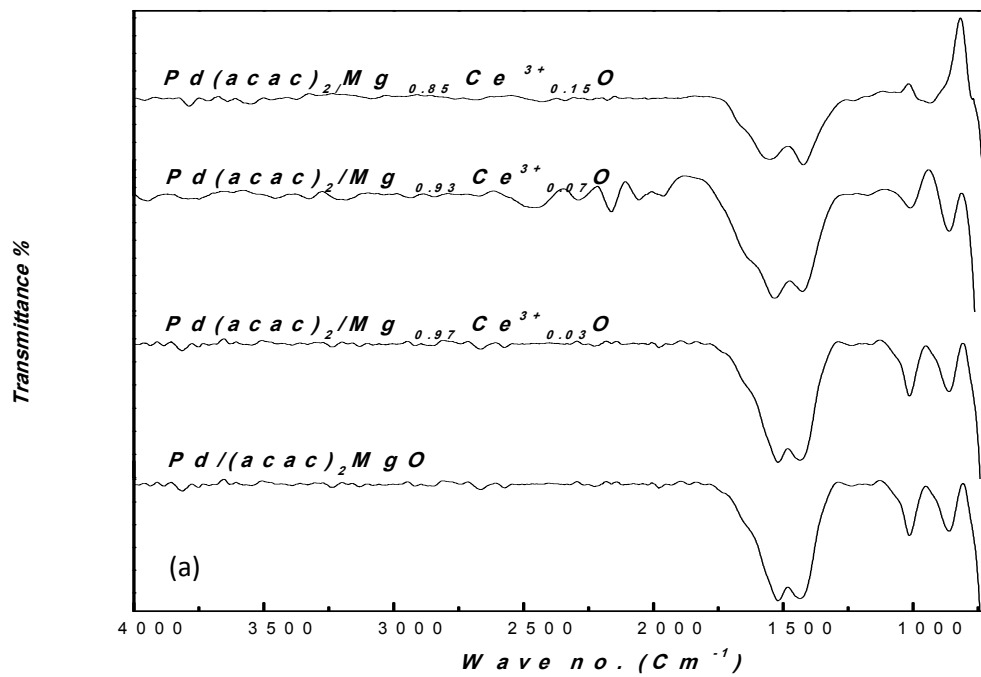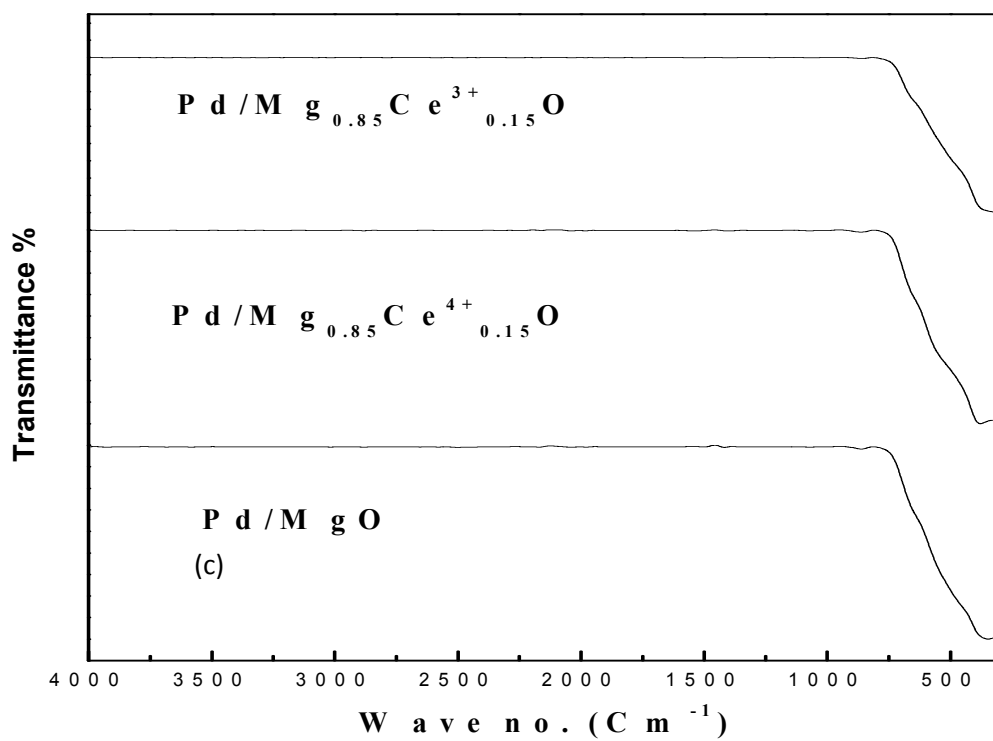
Fig. 2 FT-IR spectra for the catalysts with (a) Ce^{3+} , (b) Ce^{4+} promoter , and (c) After reduction of the catalysts.
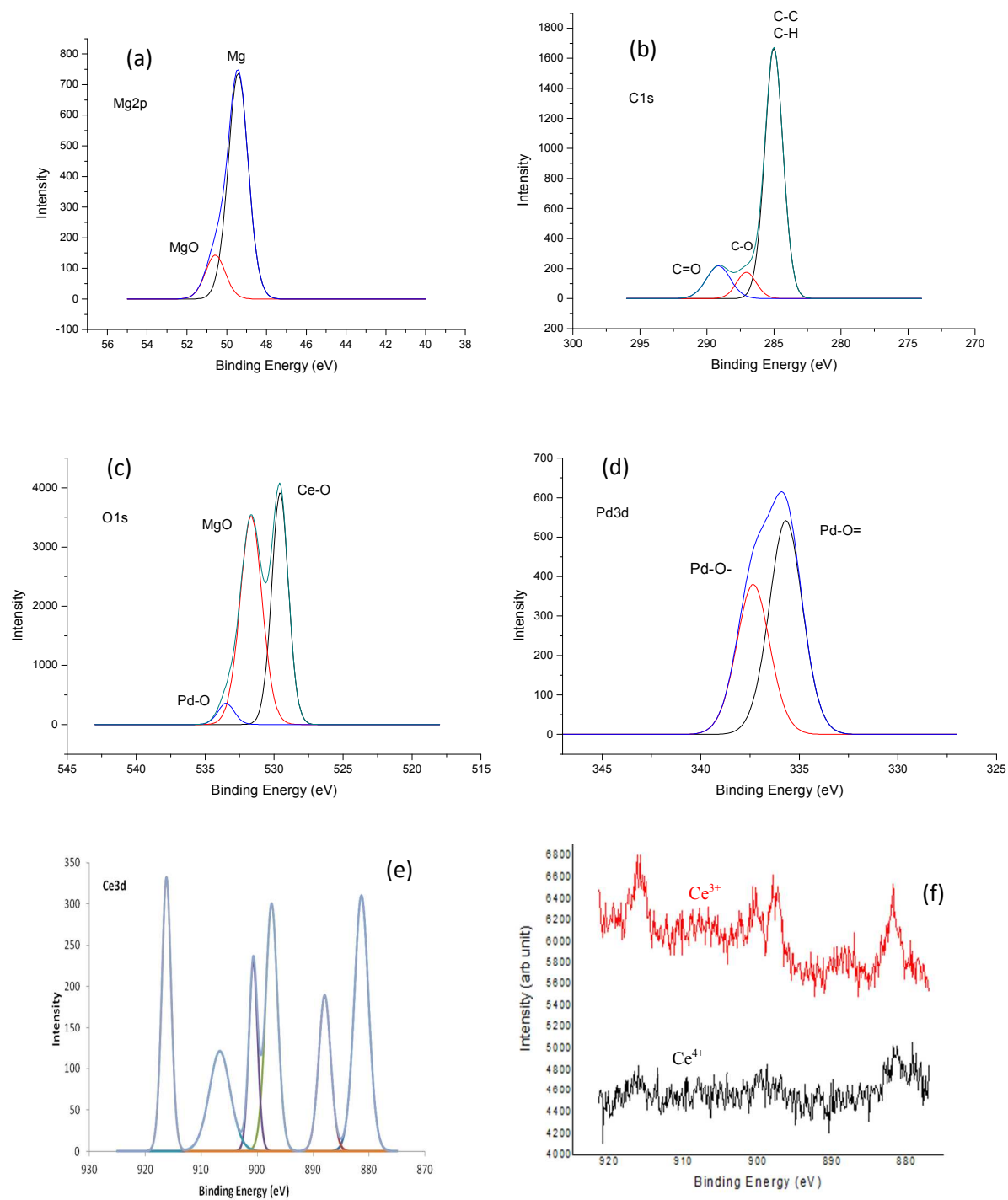
Fig. 3 XPS narrow scans of the Pd(acac)$_2$/Mg$_{0.85}$Ce$^{+3}_{0.15}$O catalyst. (a) Mg2p (b) C1s (c) O1s (d) Pd3d (e) Ce3d (f) distinguish between Ce^{3+} and Ce^{4+}.

32
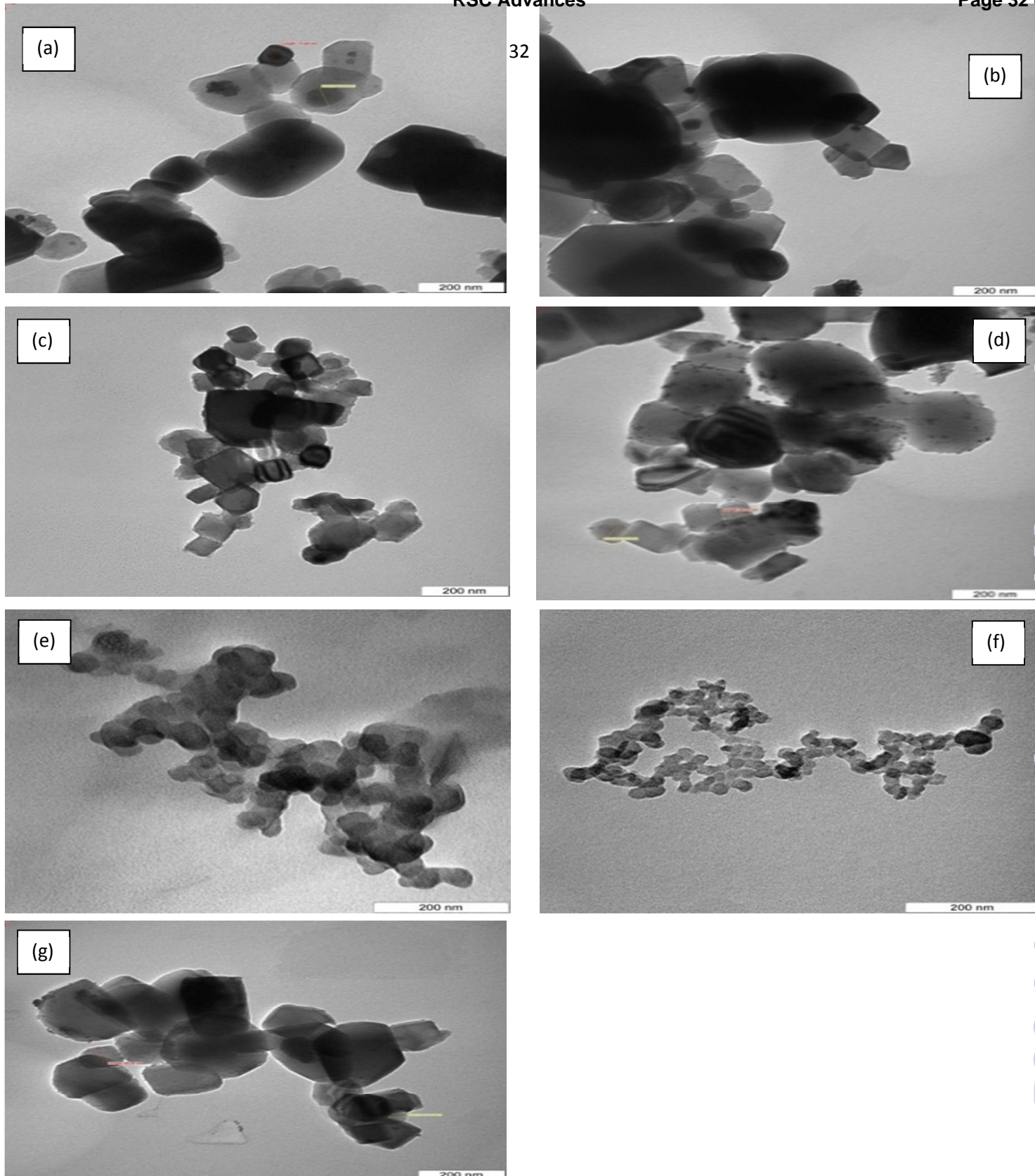
Fig. 4 TEM image of catalysts (a) Pd/MgO (b) Pd/Mg$_{0.97}$Ce$^{+3}_{0.03}$O (c) Pd/Mg$_{0.93}$Ce$^{+3}_{0.07}$O (d)

Pd/Mg$_{0.85}$Ce$^{+3}_{0.15}$O (e) Pd/Mg$_{0.97}$Ce$^{+4}_{0.03}$O (f) Pd/Mg$_{0.93}$Ce$^{+4}_{0.07}$O (g) Pd/Mg$_{0.85}$Ce$^{+4}_{0.15}$O.
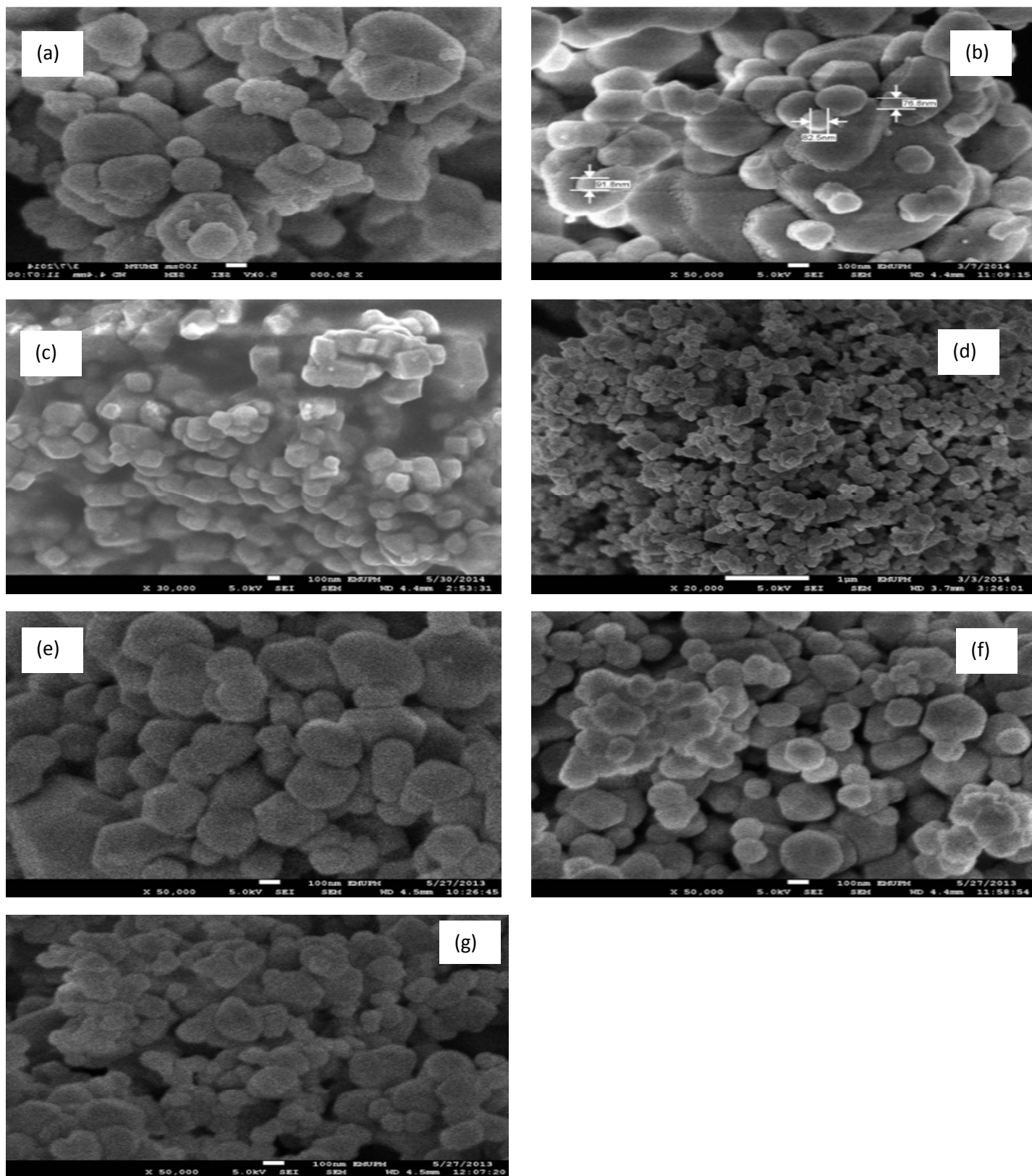
Fig. 5 FESEM image of catalysts (a) Pd/MgO (b)Pd/Mg$_{0.97}$Ce$^{+3}_{0.03}$O (c) Pd/Mg$_{0.93}$Ce$^{+3}_{0.07}$O

(d) Pd/Mg$_{0.85}$Ce$^{+3}_{0.15}$O (e) Pd/Mg$_{0.97}$Ce$^{+4}_{0.03}$O (f) Pd/Mg$_{0.93}$Ce$^{+4}_{0.07}$O (g) Pd/Mg$_{0.85}$Ce$^{+4}_{0.15}$O.
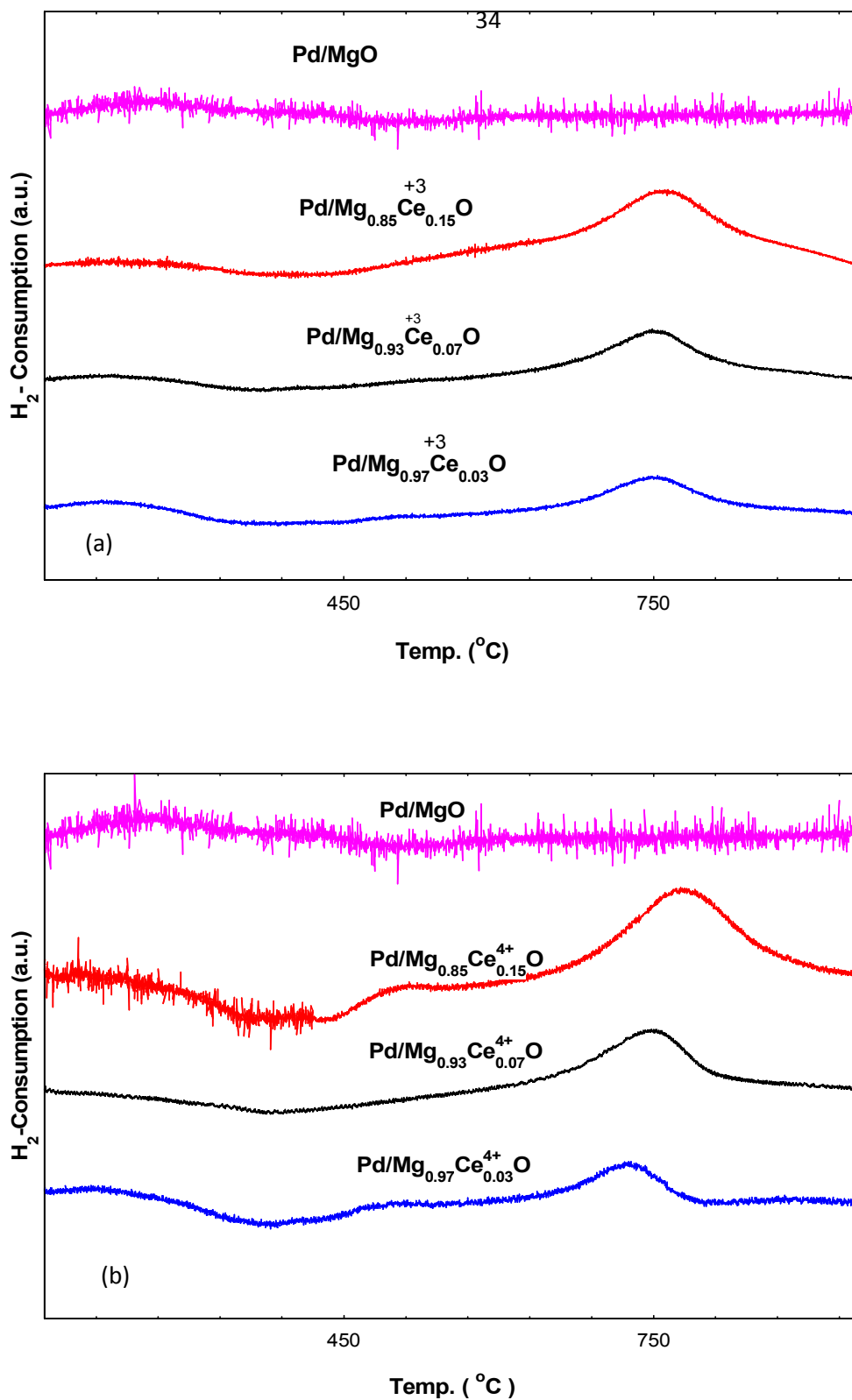
Fig. 6 TPR- H_2 profiles of catalysts (reduced in a 5 % H_2/Ar stream at a temperature ramp of 10°C/min) with (a) Ce^{3+} and (b) Ce^{4+} promoter.
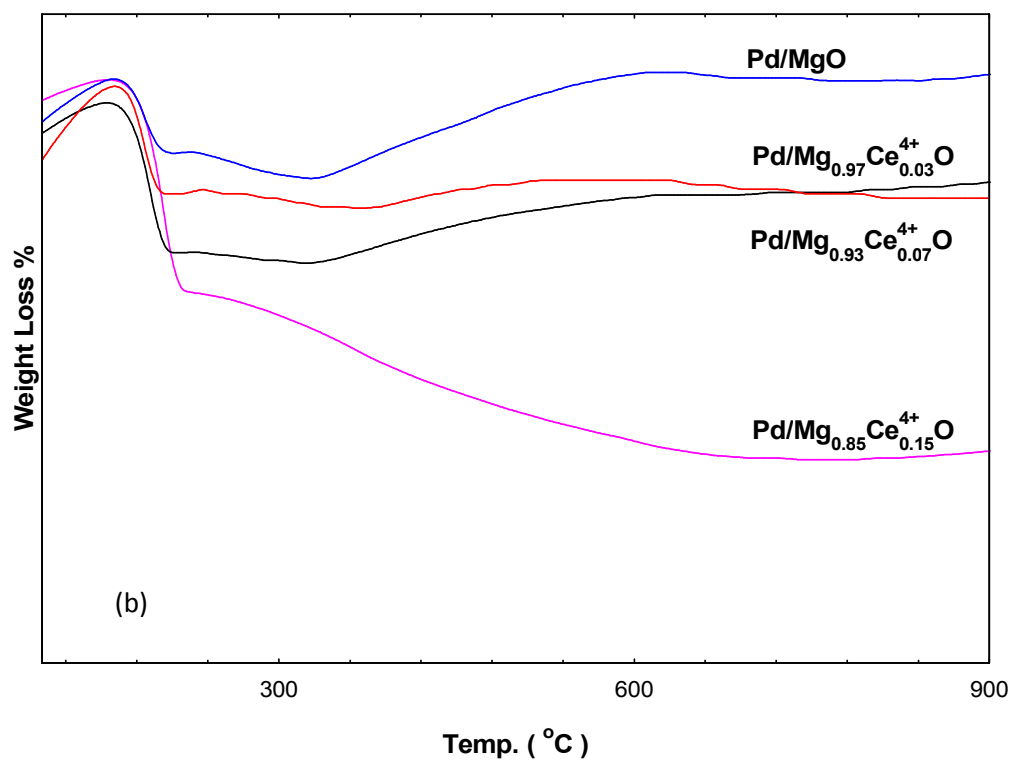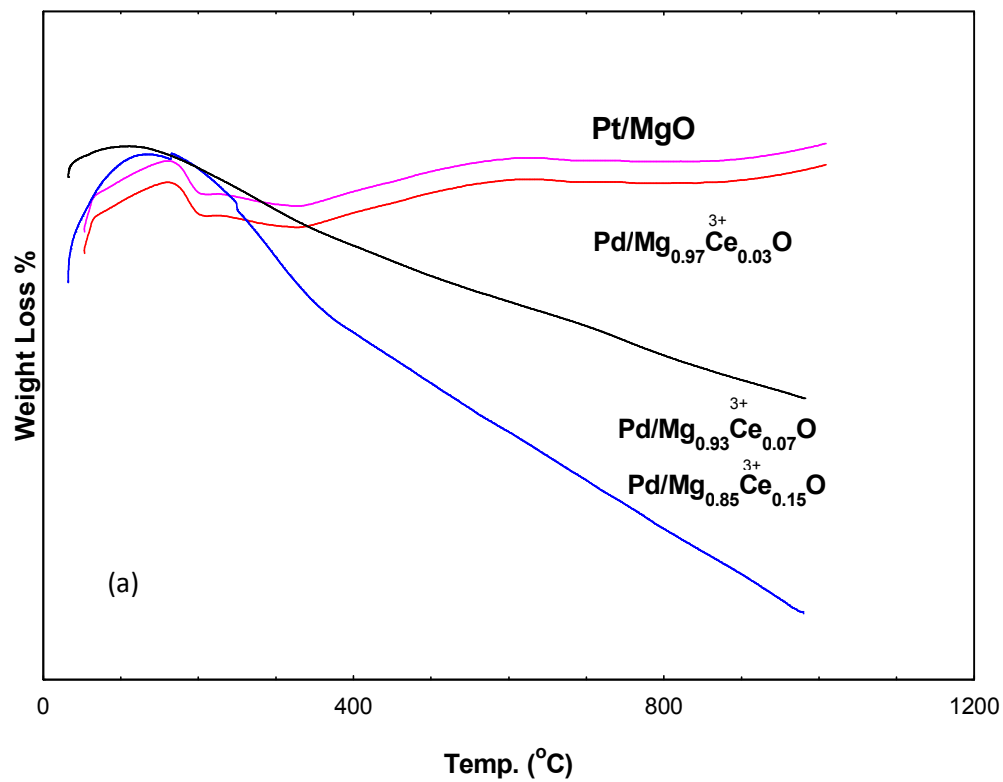
Fig. 7 TG of the catalysts with (a) Ce^{3+} and (b) Ce^{4+} promoter.
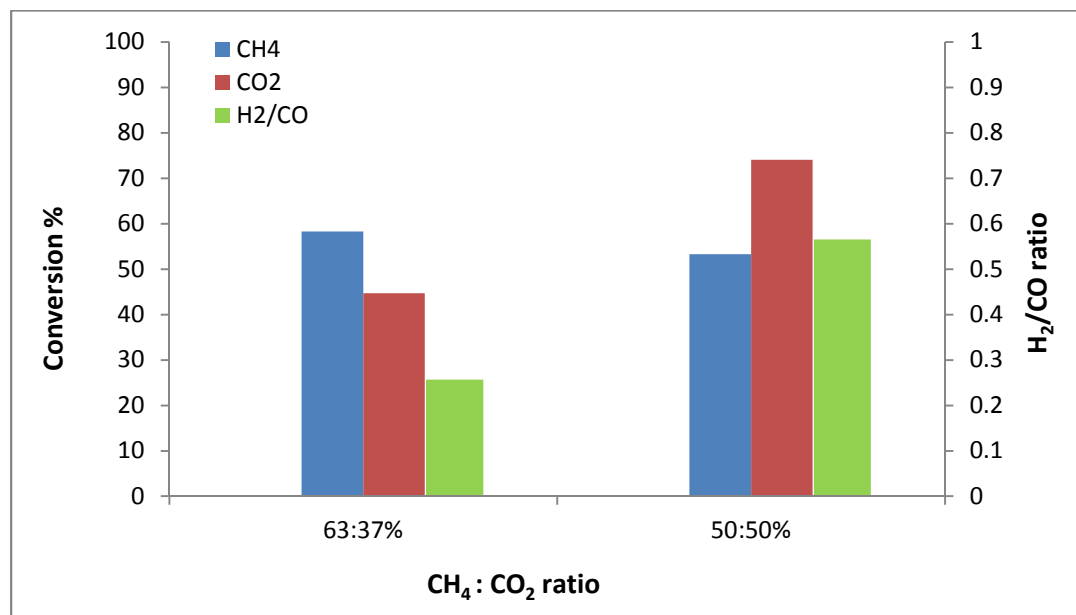
Fig. 8 The effect of changing the ratio concentration of $CH_4:CO_2$ reactant 1- 2:1 2- 1:1 over the % of their conversion and H_2/CO ratio for $Pd/Mg_{0.85}Ce^{+3}_{0.15}O$ catalyst at 900^oC.

37
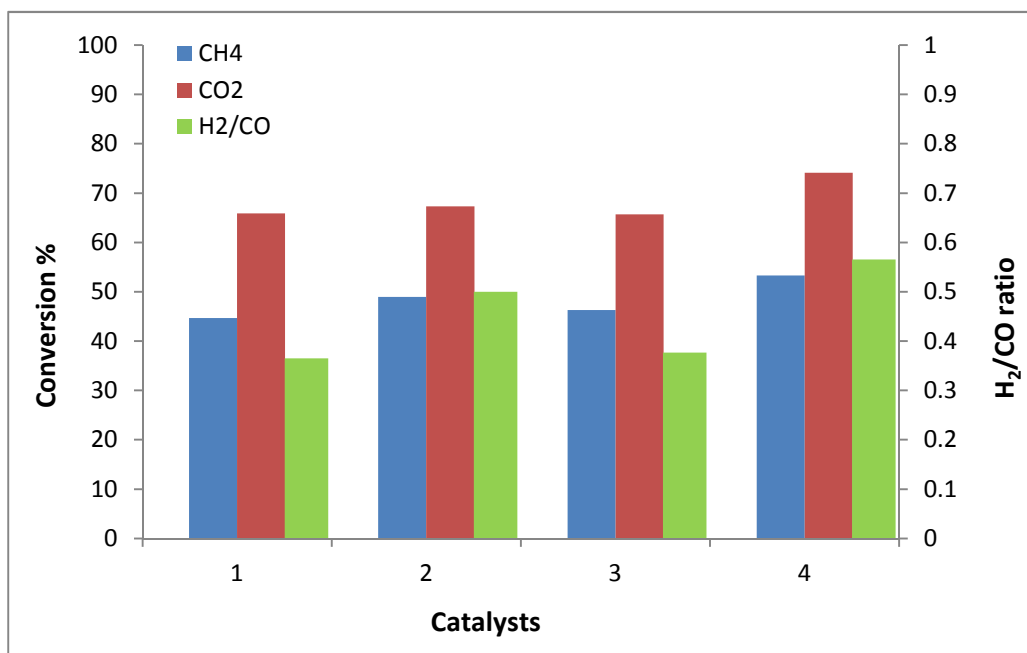
Fig. 9   The effect of using different catalysts   1) Pd/MgO,   2) Pd/Mg$_{0.97}$Ce$^{+3}_{0.03}$O,   3) Pd/Mg$_{0.93}$Ce$^{+3}_{0.07}$O, and   4) Pd/Mg$_{0.85}$Ce$^{+3}_{0.15}$O on CH$_4$, CO$_2$ conversion and H$_2$/CO ratio at 900°C for the 1:1 ratio of CH$_4$:CO$_2$.
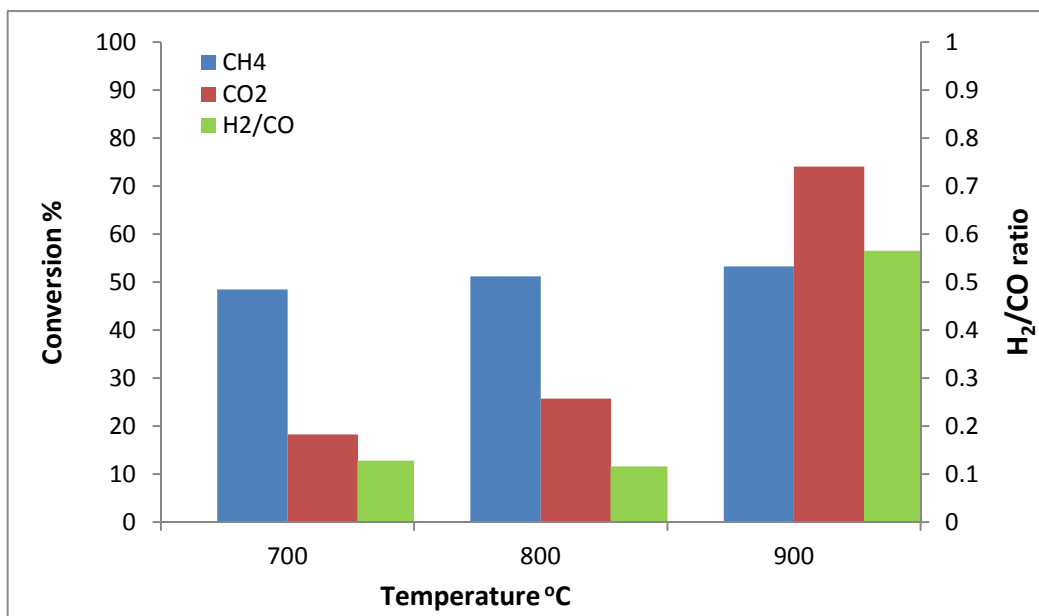
Fig. 10 The influence of temperature on the catalytic activity of the Pd/$Mg_{0.85}Ce^{+3}{}_{0.15}O$ catalyst. 1) $700^{o}C$ 2) $800^{o}C$ 3) $900^{o}C$ for the 1:1 ratio of $CH_4:CO_2$.
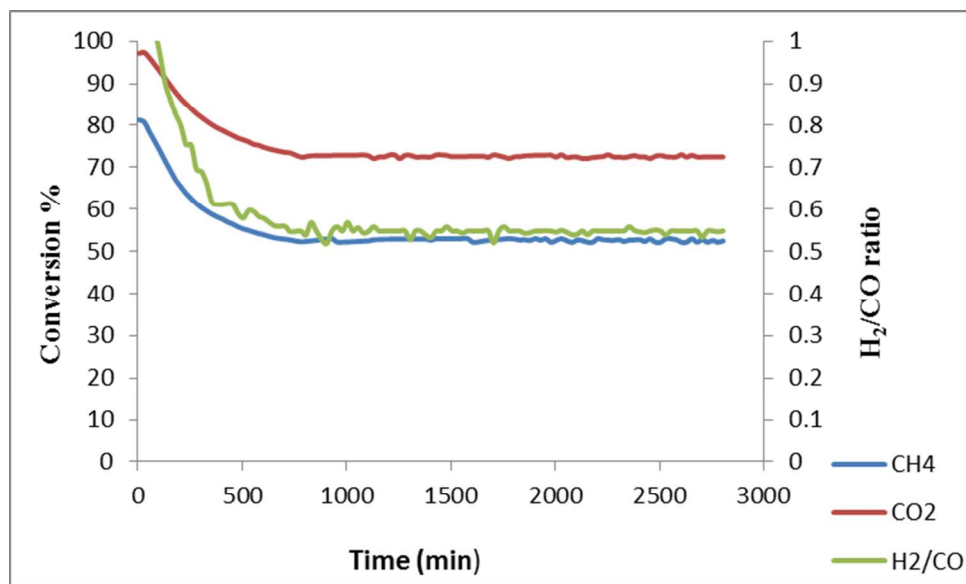
Fig. 11 Stability tests of Pd/Mg$_{0.85}$Ce$^{+3}_{0.15}$O catalysts under 900°C for the 1:1 ratio of CH$_4$:CO$_2$. for 50 h. (GHSV = 15000 ml•g cat^{-1}•h^{-1}, atmospheric pressure).

40
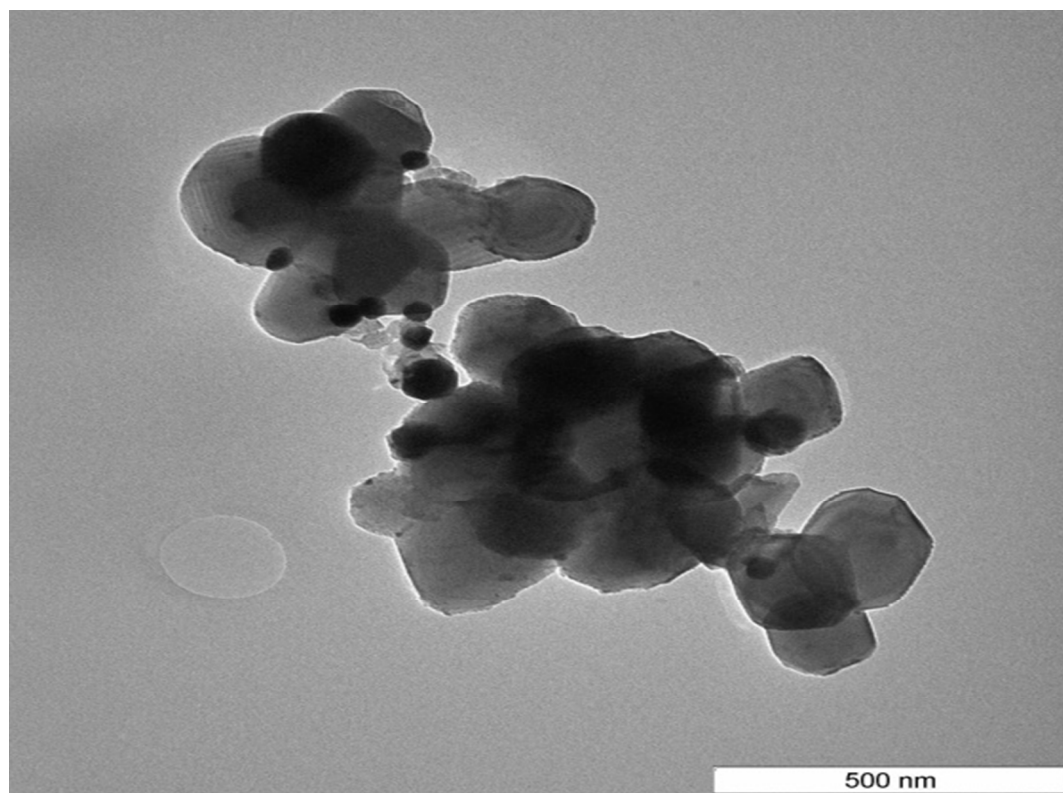
Fig. 12 TEM analysis of spent $Pd/Mg_{0.85}Ce^{+3}_{0.15}O$ catalyst after reaction: at $900^{o}C$, and CH_4/CO_2 ratio 1:1.

41
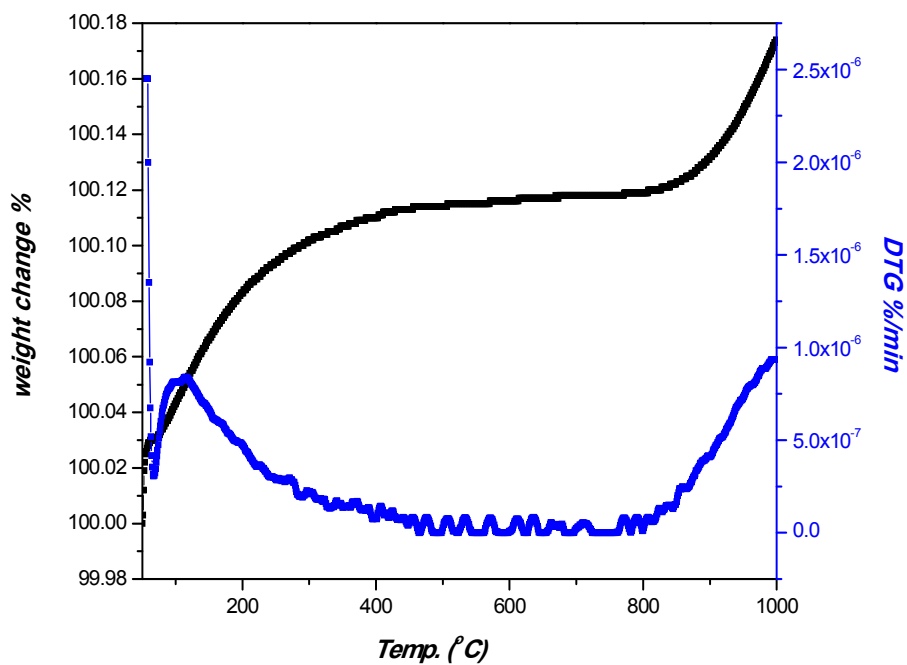
Fig. 13   TGA and DTG profiles of spent Pd/Mg$_{0.85}$Ce$^{+3}_{0.15}$O catalyst (20 mL/min O$_2$ stream under a temperature ramp of 10°C/min).

Table 1 Preparation of catalysts by prepared 0.1M solutions of the mixed promoter and support then took total weight of MgO with promoter after precipitate by 1M K_2CO_3 and calcined at 1150^oC.

Catalyst	Support (MgO) using $Mg(NO_3)_2.6H_2O$ (g)	Promoter (Ce_2O_3 or CeO_2) using $Ce(NO_3)_3.6H_2O$ or $(NH_4)_2Ce(NO_3)_6.6H_2O$ (g)	Total weight of MgO and (Ce_2O_3 or CeO_2) (g)	Impregnation of the main catalyst (1% Pd) of $Pd(acac)_2$ (g)
Pd/MgO	25.00	0.00	1	0.03
$Pd/Mg_{0.97}Ce^{+3}_{0.03}O$	24.9	1.3	1	0.03
$Pd/Mg_{0.93}Ce^{+3}_{0.07}O$	23.8	3.0	1	0.03
$Pd/Mg_{0.85}Ce^{+3}_{0.15}O$	21.8	6.5	1	0.03
$Pd/Mg_{0.97}Ce^{+4}_{0.03}O$	24.8	1.6	1	0.03
$Pd/Mg_{0.93}Ce^{+4}_{0.07}O$	23.8	3.8	1	0.03
$Pd/Mg_{0.85}Ce^{+4}_{0.15}O$	21.8	8.2	1	0.03

43

Table 2 The main textural properties of fresh catalysts

Sample name	[a] Specific surface area (m^2/g)	Pore volume cm^3/g	Pore radius ^{o}A	[b] Average crystal size nm
Pd/ MgO	15.7	0.2122	11.4	47.3
Pd/ $Mg_{0.97}Ce^{3+}_{0.03}O$	6.3	0.0946	23.6	59.2
Pd/ $Mg_{0.93}Ce^{3+}_{0.07}O$	7.5	0.1055	24.3	60.9
Pd/ $Mg_{0.85}Ce^{3+}_{0.15}O$	16.6	0.123	90.1	62.3
Pd/ $Mg_{0.97}Ce^{4+}_{0.03}O$	8.1	0.116	23.3	53.6
Pd/ $Mg_{0.93}Ce^{4+}_{0.07}O$	9.3	0.134	25.6	57.2
Pd/ $Mg_{0.85}Ce^{4+}_{0.15}O$	9.8	0.1433	30.9	58.5

a. Specific surface area calculated by BET method.

b. Determined by the Debye-Scherrer equation of the Mg (200) plane of XRD.

Table 3 TPR-H$_2$ values of the different catalysts.

Catalysts	Temp.^{o}C	Temp.^{o}C	Temp.^{o}C	Amount H$_2$-gas adsorbed(μmol/g)
Pd/MgO	247	-----	-----	224.6
Pd/Mg$_{0.97}$Ce$^{3+}_{0.03}$O	215	494	749	312.5
Pd/Mg$_{0.93}$Ce$^{3+}_{0.07}$O	213	503	754	414.9
Pd/Mg$_{0.85}$Ce$^{3+}_{0.15}$O	232	508	764	561.1
Pd/Mg$_{0.97}$Ce$^{4+}_{0.03}$O	210	498	744	267.8
Pd/Mg$_{0.93}$Ce$^{4+}_{0.07}$O	217	505	760	388.9
Pd/Mg$_{0.85}$Ce$^{4+}_{0.15}$O	233	513	776	456.5

Table 4 The catalytic results of DRM reaction for the catalysts at $900^{o}C$ for the 1:1 ratio of $CH_4:CO_2$.

Sample name	CH_4 Conversion %	CO_2 Conversion %	H_2/CO ratio
Pd/ MgO	45	66	0.3
Pd/ $Mg_{0.97}Ce^{3+}_{0.03}O$	49	67	0.5
Pd/ $Mg_{0.93}Ce^{3+}_{0.07}O$	46	66	0.4
Pd/ $Mg_{0.85}Ce^{3+}_{0.15}O$	54	74	0.6
Pd/ $Mg_{0.97}Ce^{4+}_{0.03}O$	38	53	0.2
Pd/ $Mg_{0.93}Ce^{4+}_{0.07}O$	45	58	0.5
Pd/ $Mg_{0.85}Ce^{4+}_{0.15}O$	34	54	0.2